Theory of paramagnetic scattering in highly frustrated magnets with long-range dipole-dipole interactions: The case of the $Tb_2Ti_2O_7$ pyrochlore antiferromagnet

Matthew Enjalran[1,*] and Michel J. P. Gingras[1,2,†]
[1]*Department of Physics, University of Waterloo, Ontario N2L 3G1, Canada*
[2]*Canadian Institute for Advanced Research, 180 Dundas Street West, Toronto, Ontario M5G 1Z8, Canada*
(Received 9 August 2004; published 16 November 2004)

Highly frustrated antiferromagnets composed of magnetic rare-earth moments are currently attracting much experimental and theoretical interest. Rare-earth ions generally have small exchange interactions and large magnetic moments. This makes it necessary to understand in detail the role of long-range magnetic dipole-dipole interactions in these systems, in particular, in the context of spin-spin correlations that develop in the paramagnetic phase, but are often unable to condense into a conventional long-range magnetic-ordered phase. This scenario is most dramatically emphasized in the frustrated pyrochlore antiferromagnet material $Tb_2Ti_2O_7$, which does not order down to 50 mK despite an antiferromagnetic Curie-Weiss temperature $T_{CW} \sim -20$ K. In this paper we report results from mean-field theory calculations of the paramagnetic elastic neutron scattering in highly frustrated magnetic systems with long-range dipole-dipole interactions, focusing on the $Tb_2Ti_2O_7$ system. Modeling $Tb_2Ti_2O_7$ as an antiferromagnetic $\langle 111 \rangle$ Ising pyrochlore, we find that the mean-field paramagnetic scattering is inconsistent with the experimentally observed results. Through simple symmetry arguments we demonstrate that the observed paramagnetic correlations in $Tb_2Ti_2O_7$ are precluded from being generated by any spin Hamiltonian that considers only Ising spins, but are qualitatively consistent with Heisenberg-like moments. Explicit calculations of the paramagnetic scattering pattern for both $\langle 111 \rangle$ Ising and Heisenberg models, which include finite single-ion anisotropy, support these claims. We offer suggestions for reconciling the need to restore spin isotropy with the Ising-like structure suggested by the single-ion properties of Tb^{3+}.

DOI: 10.1103/PhysRevB.70.174426 PACS number(s): 75.10.Hk, 75.25.+z, 75.30.Gw, 75.40.Cx

I. INTRODUCTION

The pyrochlore oxides, with the general formula $A_2B_2O_7$, have attracted a great deal of attention over the last decade because the combination of lattice geometry and chemical composition allows for a plethora of interesting physical phenomena in these materials.[1–3] The A and B sites reside on two distinct interpenetrating pyrochlore networks of corner-sharing tetrahedra, Fig. 1. Since A^{3+} can be either a magnetic rare-earth or a nonmagnetic transition metal and B^{4+} can be a transition metal with or without a moment, there are numerous possibilities to study insulating and itinerant magnetic models in a geometrically frustrated environment. Experimentally, long-range magnetic-ordered states,[4–6] magnetic phases (e.g., spin glass,[7–11] spin ice,[3,12–14] spin liquid[15,16]), anomalous Hall effect,[17] metallic properties,[18] and superconductivity[19,20] have been observed in the pyrochlore oxides. Materials with the pyrochlore-related spinel structure have also attracted much attention recently. Heavy fermion physics has been observed in the *d*-electron LiV_2O_4 compound.[21] In the spinel antiferromagnet $ZnCr_2F_4$, a spin-Peierls-like transition has been observed[22] at low temperatures and a protectorate of weakly interacting spin directors slightly above the spin-Peierls transition temperature.[23]

In insulating rare-earth magnetic pyrochlores, the magnetic rare-earth ions often have large dipole moments, i.e., $\mu \gg 1\mu_B$ and small Heisenberg exchange interactions. In such a situation, long-range dipole-dipole interactions are a significant contribution to the Hamiltonian. As well, a large single-ion anisotropy interaction is also often present. For example, crystal fields produce an effective Ising doublet at the rare-earth ion site, A^{3+}, in the $Ho_2Ti_2O_7$ (Ref. 24), $Dy_2Ti_2O_7$ (Ref. 24), $Tb_2Ti_2O_7$ (Refs. 24 and 25), and $Yb_2Ti_2O_7$ (Ref. 26) materials. An energy gap separates the ground-state doublet from the lowest-lying excited states with the Ising quantization axis coinciding with the local

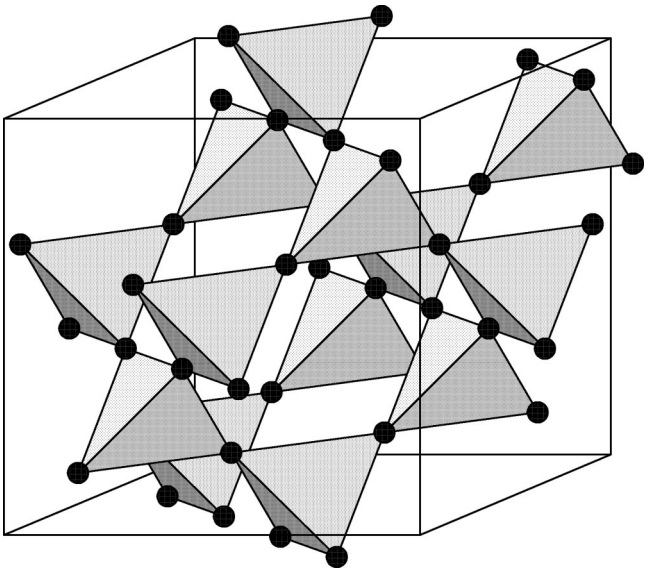

FIG. 1. The pyrochlore lattice structure. The lattice is constructed from a network of corner sharing tetrahedra in which each tetrahedron resides at an fcc Bravais lattice point. A cubic cell contains 4 tetrahedra or 16 atoms.

 ©2004 The American Physical Society

cubic ⟨111⟩ directions,[24,25] i.e., the quantization axis points toward the center of the tetrahedral-basis unit cell. Most noticeably, this strong local ⟨111⟩ Ising-axis anisotropy has been found responsible for endowing frustration to the pyrochlore lattice in the presence of effective nearest-neighbor ferromagnetic (FM) interactions.[12,27,28] From a statistical mechanics point of view, a FM ⟨111⟩ Ising pyrochlore model is equivalent to a model for disordered water ice I_h, where both magnetic[12] and water-ice[29–31] models possess macroscopic degeneracy. Recent experiments on the magnetic systems $Dy_2Ti_2O_7$ (Ref. 13) and $Ho_2Ti_2O_7$ (Refs. 32 and 33), so-called spin-ice materials, reveal a residual entropy in agreement with the prediction for water ice.[31] In contrast, nearest-neighbor antiferromagnetic (AFM) interactions in a ⟨111⟩ Ising-pyrochlore model are nonfrustrated;[25,27,28,34] therefore, such a model is expected to order at a temperature set by the nearest-neighbor energy scale, i.e., $T_N \approx J_{\mathrm{nn}}^{\mathrm{eff}}/k_{\mathrm{B}}$. A candidate AFM ⟨111⟩ pyrochlore material is $Tb_2Ti_2O_7$, where a noncollinear long-range ordered state is expected at $T_N \approx 1$ K.[25,35] However, experiments indicate the material fails to order down to $T=50$ mK,[15,16] despite an antiferromagnetic Curie-Weis temperature, $\theta_{\mathrm{CW}} \sim -20$ K, making this system, thus far, one of the cleanest realizations of a spin liquid in a three-dimensional system. The mechanism responsible for $Tb_2Ti_2O_7$ failing to order down to such low temperatures has not yet been resolved.[36]

In $Tb_2Ti_2O_7$, the energy gap between the ground-state doublet and the first excited-state doublet is $\Delta \approx 20$ K (Refs. 24 and 25). The size of anisotropy gap here is an order-of-magnitude smaller than what is observed in the spin-ice materials, $\Delta = 250-350$ K (Ref. 24), and is comparable to θ_{CW} for $Tb_2Ti_2O_7$. Consequently, in early theoretical work on $Tb_2Ti_2O_7$, a ⟨111⟩ Ising model was assumed and a noncollinear long-rang ordered state with zero net moment about each until tetrahedron ($\mathbf{q}=\mathbf{0}$ state) was predicted at $T \approx 1$ K (Refs. 25 and 35). However, muon spin-relaxation measurements indicate a dynamically fluctuating state at all experimentally achievable temperatures, which recent results pushed down below 50 mK (Ref. 16). In contrast, some static susceptibility data suggest a spin-glass state at these temperatures.[37] Despite the experimental evidence that the magnetic single-ion ground state of Tb^{3+} is an Ising doublet,[24,25] several experimental groups have used simple Heisenberg-type models [which for the pyrochlore lattice is paramagnetic down to $T \to 0^+$ (Refs. 38–40)] to obtain qualitative agreement with the observed paramagnetic (PM) scattering pattern.[41,42] Finally, we note that high-pressure neutron-scattering experiments on $Tb_2Ti_2O_7$ find a transition to long-range order at a temperature in excess of 1 K for an applied pressure larger than 2 GPa,[43] but the magnetic structure has not been determined. In summary, there is currently ambiguity even as to the nature of the paramagnetic correlations developing in $Tb_2Ti_2O_7$ at temperatures above θ_{CW}. This is an important issue since very recent neutron-scattering measurements on a single crystal of $Tb_2Ti_2O_7$ down to 50 mK have found that the scattered intensity in reciprocal space remains essentially unchanged (i.e., frozen out) when going from the paramagnetic temperature of 10 K down to 50 mK (Ref. 16). It would therefore appear that a first requirement to make theoretical progress in understanding the spin-liquid state in $Tb_2Ti_2O_7$ would be to understand the nature of the paramagnetic spin—spin correlations. It is the aim of this paper to shed some light on the paramagnetic correlations of this material.

In this article, we use mean-field theory (MFT) to investigate the paramagnetic spin-spin correlations of a ⟨111⟩ Ising dipolar model pertinent to $Tb_2Ti_2O_7$ as well as a finite Ising anisotropy model. In MFT, the PM regime is realized for temperatures above an energy scale set by the mean-field (MF) critical mode, i.e., $T > T_c^{\mathrm{MF}} \equiv \lambda_c^{\mathrm{MF}}/n$, where T is temperature in units of k_{B}, n is the number of spin components, and λ_c^{MF} represents the mean-field global maximum eigenvalue of the $\mathbf{q}$-dependent susceptibility. As the temperature approaches T_c^{MF}, one expects the critical mode to control the spin-spin correlations. A clear understanding of this critical mode softening relies on an accurate treatment of all interactions in the Hamiltonian. The long-range dipole-dipole interactions are our main concern. Our major results are the following: We establish, on symmetry grounds and through calculations, that the observed PM neutron scattering is inconsistent with a local ⟨111⟩ Ising dipolar model. Calculations performed for an anisotropic Heisenberg pyrochlore model yield good agreement with experiment and thus support the claim that at least a partial restoration of spin isotropy occurs in $Tb_2Ti_2O_7$.

We also have in mind a broader perspective in presenting the enclosed work and detailed derivation of the mean-field formulation of the structure factor $S(\mathbf{q})$ for highly frustrated magnets. In the past few years, there have been a number of interesting and puzzling thermodynamic data and neutron-scattering results on highly frustrated magnets. Examples include the antiferromagnetic $Gd_3Ga_5O_{12}$ garnet (referred to as GGG),[44–49] the pyrochlore antiferromagnet $Gd_2Ti_2O_7$ (Refs. 4–6, 50, and 51), and the pyrochlore ferromagnet $Yb_2Ti_2O_7$ (Refs. 26 and 52). The experimental results on these systems, which will be discussed in more detail in Section IV, raise a common issue: To further our current understanding of a number of highly frustrated magnets, including quantum fluctuations,[53] we need to have a clear and quantitative understanding of the predominant correlations that initially develop out of the paramagnetic state as the materials are cooled. The mean-field theory described herein is an approach to formulate such a program. For concreteness, this paper focuses on the specific cases of insulating pyrochlore oxides with local ⟨111⟩ Ising axis anisotropy. It is straightforward to use the formalism herein to tackle the frustrated dipolar systems described above as well as others.

The outline of the paper is as follows: In Section II a condensed description of the MFT formalism of neutron scattering for the anisotropic Heisenberg and ⟨111⟩ Ising pyrochlores is presented. We give the MFT results for the paramagnetic scattering of $Tb_2Ti_2O_7$ in Section III. Our mean-field data are also compared to Monte Carlo results for the paramagnetic $S(\mathbf{q})$. Section IV discusses the need to relax the ⟨111⟩ Ising constraint to allow for transverse fluctuations in $Tb_2Ti_2O_7$. For completeness, we include several detailed appendixes. In Appendix A, the variational MFT is discussed and the equations for elastic neutron scattering are derived in detail. An alternate approach—a high-temperature series expansion—to the equations for neutron scattering is pre-

TABLE I. Our convention for vectors: The $\mathbf{r}^a$ define the basis vectors and $\hat{z}^a$ define the local $\langle 111\rangle$ anisotropy axes for spins on the pyrochlore lattice. The size of the corresponding cubic cell is given by $\overline{a}$ and contains 16 atoms. Vectors $\hat{n}^u$ represent the global Cartesian-basis vectors.

$\mathbf{r}^{(1)}$	$\overline{a}/4$ (0,0,0)	$\hat{z}^{(1)}$	$1/\sqrt{3}$ (1,1,1)	$\hat{n}^{(1)}$	(1,0,0)
$\mathbf{r}^{(2)}$	$\overline{a}/4$ (1,1,0)	$\hat{z}^{(2)}$	$1/\sqrt{3}$ (−1,−1,1)	$\hat{n}^{(2)}$	(0,1,0)
$\mathbf{r}^{(3)}$	$\overline{a}/4$ (1,0,1)	$\hat{z}^{(3)}$	$1/\sqrt{3}$ (−1,1,−1)	$\hat{n}^{(3)}$	(0,0,1)
$\mathbf{r}^{(4)}$	$\overline{a}/4$ (0,1,1)	$\hat{z}^{(4)}$	$1/\sqrt{3}$ (1,−1,−1)		

sented in Appendix B. The derivation of the Ewald equations for the **q**-dependent dipole-dipole Hamiltonian is given in Appendix C. Appendix D contains a detailed discussion of the symmetry-allowed scattering patterns for $\langle 111\rangle$ Ising and Heisenberg pyrochlores. We note that other authors have discussed various aspects of the mean-field theory[39,54–57] and Ewald[58–61] derivations presented in Appendixes A and C, respectively. Our purpose here is to provide a self-contained reference for the application of the Ewald method within a mean-field formalism, connecting at times with results from earlier work,[56] and which will be useful to other researchers who wish to study frustrated magnetic systems with non-Bravais lattice geometries and allowing for an array of possible spin symmetries and interactions.

II. MEAN-FIELD THEORY OF NEUTRON SCATTERING IN THE PYROCHLORES

In this section, we present the models and provide an outline of the derivation of the mean-field equations for the neutron-scattering cross section, $d\sigma(Q)/d\Omega$, for classical spins on the pyrochlore lattice. The resulting equations are only applicable in the disordered paramagnetic regime of the model Hamiltonians. Our derivation is performed for the general anisotropic Heisenberg model because it has broad appeal to the study of many highly frustrated magnetic systems. Our method is best described as variational mean-field theory[54] (VMFT) (which is equivalent to a Gaussian approximation of the free energy) and has been used to study frustrated magnetic systems.[39,56,57] The details of VMFT and its application to the scattering cross section are presented in Appendix A. We remind the reader that MFT corresponds to a partial resummation of an infinite number of terms in the high-temperature series expansion for the **q**-dependent susceptibility $\chi(\mathbf{q})$. In particular, the correlations $\langle \mathbf{S}(0)\cdot\mathbf{S}(r)\rangle$ are correctly treated to order $\beta=1/T$ [or $\chi(\mathbf{q})$ to $1/T^2$] in MFT. This is demonstrated in Appendix B, where scattering cross-section equations are derived via a high-temperature series expansion.

A. Models

The pyrochlore lattice, Fig. 1, is a non-Bravais lattice that we describe as a fcc lattice with a four-atom unit cell. The positions of the fcc Bravais lattice points, which coincide with a corner point on the tetrahedral basis, are denoted by $\mathbf{R}_i$. The four atoms that form the tetrahedron at each fcc point (and represent different sublattices) are labeled by $\mathbf{r}^a$. Hence, the position of a site in the pyrochlore lattice is given by $\mathbf{R}_i^a=\mathbf{R}_i+\mathbf{r}^a$. Table I lists our convention for the tetrahedral-basis coordinates $\mathbf{r}^a$. The most general Hamiltonian for rare-earth spins on the pyrochlore lattice is a Heisenberg model with nearest-neighbor exchange, dipole-dipole, and single-ion anisotropy (with a local $\langle 111\rangle$ orientation) energies,

$$H_H = -J\sum_{\langle (i,a),(j,b)\rangle}\mathbf{S}_i^a\cdot\mathbf{S}_j^b-\Delta\sum_{i,a}(\hat{z}^a\cdot\mathbf{S}_i^a)^2 + D_{\mathrm{dd}}\sum_{(i,a)>(j,b)}\left[\frac{\mathbf{S}_i^a\cdot\mathbf{S}_j^b}{|\mathbf{R}_{ij}^{ab}|^3}-\frac{3(\mathbf{S}_i^a\cdot\mathbf{R}_{ij}^{ab})(\mathbf{S}_j^b\cdot\mathbf{R}_{ij}^{ab})}{|\mathbf{R}_{ij}^{ab}|^5}\right]. \tag{1}$$

The unit vector $\hat{z}^a$ represents the local $\langle 111\rangle$ quantization axis that points toward the center of a tetrahedron. Table I defines our convention for $\hat{z}^a$. The spins $\mathbf{S}_i^a$ have unit length and full $O(3)$ symmetry, $\mathbf{R}_{ij}^{ab}=\mathbf{R}_i^a-\mathbf{R}_j^b$ is the vector separation between spins $\mathbf{S}_i^a$ and $\mathbf{S}_j^b$, and J and Δ define the exchange and single-ion energy scales, respectively. The convention established in Eq. (1) defines $J>0$ as FM and $J<0$ as AFM exchange energies. The dipolar energy scale is set by $D_{\mathrm{dd}}\equiv DR_{\mathrm{nn}}^3$, where

$$D=\frac{\mu_{\mathrm{o}}}{4\pi}\frac{\mu^2}{R_{\mathrm{nn}}^3},$$

μ is the moment on the rare-earth ion, and R_{nn} is the nearest-neighbor distance.

The $\langle 111\rangle$ Ising dipolar model for the pyrochlore lattice[35] is obtained by considering the limit of large Ising anisotropy in Eq. (1) ($\Delta/|J|\gg 1$ and $\Delta/D\gg 1$). The low-energy physics of this system is modeled by the Hamiltonian,

$$H_I = -J\sum_{\langle (i,a),(j,b)\rangle}(\hat{z}^a\cdot\hat{z}^b)\sigma_i^a\sigma_j^b + D_{\mathrm{dd}}\sum_{(i,a)>(j,b)}\left(\frac{(\hat{z}^a\cdot\hat{z}^b)}{|\mathbf{R}_{ij}^{ab}|^3}-\frac{3(\hat{z}^a\cdot\mathbf{R}_{ij}^{ab})(\hat{z}^b\cdot\mathbf{R}_{ij}^{ab})}{|\mathbf{R}_{ij}^{ab}|^5}\right)\sigma_i^a\sigma_j^b. \tag{2}$$

By low-energy physics we mean that the single-ion term in Eq. (1) is removed and the spins are restricted to lie along the local $\langle 111\rangle$ quantization axis, i.e., $\mathbf{S}_i^a=\hat{z}^a\sigma_i^a$ with $\sigma_i^a=\pm 1$. If one were to truncate the dipolar sum in Eq. (2) at nearest-neighbor distances, then the following effective nearest-neighbor energy scale could be defined:

$$J_{\mathrm{nn}}^{\mathrm{eff}}\equiv J_{\mathrm{nn}}+D_{\mathrm{nn}}, \tag{3}$$

where $J_{\mathrm{nn}}=J/3$ and $D_{\mathrm{nn}}=5D/3$. For FM effective nearest-neighbor exchange, $J_{\mathrm{nn}}^{\mathrm{eff}}>0$ setting all dipolar interactions be-

yond nearest-neighbor to zero, one has the nearest-neighbor spin-ice model of Harris *et al.* (Refs. 12 and 27). If the nearest-neighbor interactions $J_{\rm nn}^{\rm eff}$ are AFM, then the model possesses a unique ordered state ($\mathbf{q}=\mathbf{0}$, all-in all-out state) at temperatures on the order of $|J_{\rm nn}^{\rm eff}|$ (Refs. 25, 27, 28, and 34). The transition between the spin-ice and $\mathbf{q}=\mathbf{0}$ phases occurs at $J_{\rm nn}/D_{\rm nn}=-1.0$. When dipole-dipole sum is extended to long-range distances, the transition between the $\mathbf{q}=\mathbf{0}$ and the spin-ice states shifts to $J_{\rm nn}/D_{\rm nn} \cong -0.908$. Hence, long-range dipolar interactions favor the $\mathbf{q}=\mathbf{0}$ AFM phase slightly.[35]

B. Mean-field theory

We are interested in calculating the elastic neutron-scattering cross section for both Heisenberg and ⟨111⟩ Ising spins on the pyrochlore lattice at the mean-field level. Therefore, we use the general anisotropic Hamiltonian H_H as the starting point for MFT and include a local, fictitious field term, $|\mathbf{h}|=|\mathbf{h}_i^a|$, (where at the end of the calculation $\mathbf{h}_i^a \to \mathbf{0}$),

$$H_H = -\tfrac{1}{2}\sum_{i,j}\sum_{a,b}\sum_{u,v}\mathcal{J}_{uv}^{ab}(i,j)S_i^{a,u}S_j^{b,v} - \sum_{i,a,u} h_i^{a,u}S_i^{a,u}, \qquad (4)$$

where

$$\mathcal{J}_{uv}^{ab}(i,j) = J\delta_{R_{ij}^{ab},R_{nn}}(\hat{n}^u\cdot\hat{n}^v) + \Delta\,\delta_{i,j}\delta^{a,b}(\hat{z}^a\cdot\hat{n}^u)(\hat{z}^b\cdot\hat{n}^v) - D_{dd}\left(\frac{(\hat{n}^u\cdot\hat{n}^v)}{|R_{ij}^{ab}|^3} - \frac{3(\hat{n}^u\cdot\mathbf{R}_{ij}^{ab})(\hat{n}^v\cdot\mathbf{R}_{ij}^{ab})}{|\mathbf{R}_{ij}^{ab}|^5}\right). \qquad (5)$$

In the notation of this general model, the spin vectors are represented by $\mathbf{S}_i^a=\hat{n}^{(1)}S_i^{a,1}+\hat{n}^{(2)}S_i^{a,2}+\hat{n}^{(3)}S_i^{a,3}$, where the unit vectors $\hat{n}^u$ are the global Cartesian unit vectors, see Table I, and $S_i^{a,u}$ is the uth component of spin. The sum in Eq. (4) does not include terms with $\mathbf{R}_{ij}^{ab}=0$. For ⟨111⟩ Ising spins, one begins with H_I, Eq. (2), and adds the field term $-\Sigma_{i,a}(\mathbf{h}_i^a\cdot\hat{z}^a)\sigma_i^a$. The resultant interaction parameter $\mathcal{J}^{ab}(i,j)$ does not include the spin components.

The general expression for the mean-field free energy is as follows:

$$F_\rho = \mathrm{Tr}\{\rho H_H\} + T\mathrm{Tr}\{\rho\ln\rho\} = \langle H_H\rangle_\rho + T\langle\ln\rho\rangle_\rho, \qquad (6)$$

where ρ is the many-body density matrix and Tr represents a trace over the states of ρ. A mean-field form for F_ρ is obtained by first expressing the many-body density matrix as a product of single-particle density matrices $\rho(\{\mathbf{S}_i^a\}) = \Pi_{i,a}\rho_i^a(\mathbf{S}_i^a)$, followed by minimizing F_ρ with respect to ρ_i^a (the variational parameters) subject to the constraints $\mathrm{Tr}\{\rho_i^a\}=1$ and $\mathrm{Tr}\{\rho_i^a\mathbf{S}_i^a\}=\mathbf{m}_i^a$, where $\mathbf{m}_i^a$ is the local, vector order parameter. For Ising spins, $\mathbf{m}_i^a$ has only one component, m_i^a. Next, the resulting mean-field free energy is transformed to momentum space by applying the definitions,

$$m_i^{a,u} = \sum_{\mathbf{q}} m_{\mathbf{q}}^{a,u}\mathrm{e}^{-\imath\mathbf{q}\cdot\mathbf{R}_i^a}, \qquad (7)$$

$$\mathcal{J}_{uv}^{ab}(i,j) = \frac{1}{N_{\rm cell}}\sum_{\mathbf{q}}\mathcal{J}_{uv}^{ab}(\mathbf{q})\mathrm{e}^{\imath\mathbf{q}\cdot R_{ij}^{ab}}, \qquad (8)$$

where $N_{\rm cell}$ is the number of fcc Bravais lattice points. We note that the above convention for the Fourier transform, which employs the position of the spin $\mathbf{R}_i^a$, results in a real symmetric $\mathbf{q}$-dependent interaction matrix $\mathcal{J}(\mathbf{q})$, 12×12 for Heisenberg and 4×4 for Ising spins. An alternate convention for the Fourier transform uses $\mathbf{R}_i$, the Bravais lattice points, instead of $\mathbf{R}_i^a$ and yields a complex $\mathcal{J}(\mathbf{q})$; refer to Appendix A for details. For a non-Bravais lattice, the interaction matrix is not fully diagonalized by a Fourier transform. Hence, to completely diagonalize $\mathcal{J}(\mathbf{q})$, one must transform the $\mathbf{q}$-dependent variables $\mathbf{m}_{\mathbf{q}}^a$ to normal mode variables. In component form, the normal mode transformation is given by

$$m_{\mathbf{q}}^{a,u} = \sum_{\alpha=1}^{4}\sum_{\mu=1}^{3} U_{u,\mu}^{a,\alpha}(\mathbf{q})\phi_{\mathbf{q}}^{\alpha,\mu}, \qquad (9)$$

where the indices (α,μ) label the normal modes (12 for Heisenberg spins) and $\{\phi_{\mathbf{q}}^{\alpha,\mu}\}$ are the amplitudes of the normal modes. In matrix form, $U(\mathbf{q})$ is the unitary matrix that diagonalizes $\mathcal{J}(\mathbf{q})$ in the spin$\otimes$sublattice space with eigenvalues $\lambda(\mathbf{q})$. Hence, $U_{u,\mu}^{a,\alpha}(\mathbf{q})$ represents the (a,u) component of the (α,μ) eigenvector at $\mathbf{q}$ with eigenvalue $\lambda_\mu^\alpha(\mathbf{q})$. Finally, the mean-field free energy to quadratic order in the normal modes reads,

$$\mathcal{F}_\rho(T) = \tfrac{1}{2}\sum_{\mathbf{q},\alpha,\mu}\left[nT-\lambda_\mu^\alpha(\mathbf{q})\right]|\phi_{\mathbf{q}}^{\alpha,\mu}|^2 - T\sum_{\mathbf{q},\alpha,\mu}\tilde{h}_{\mathbf{q}}^{\alpha,\mu}\phi_{-\mathbf{q}}^{\alpha,\mu}, \qquad (10)$$

where $\mathcal{F}_\rho(T)=F_\rho(T)/N_{\rm cell}$, $\tilde{h}_{\mathbf{q}}^{\alpha,\mu}\propto\mathbf{h}_{\mathbf{q}}^{a,u}/T$, T is the temperature in units of $k_{\rm B}$, and $n=3$ for Heisenberg spins. Note, in order to consider the Ising case, the indices u and μ are dropped from Eq. (10) and $n=1$. We have also dropped a constant from the expression for $\mathcal{F}_\rho(T)$, refer to Appendix A.

The neutron-scattering cross section for unpolarized neutrons in the dipole approximation is given by the general expression,[62,63]

$$\frac{d\sigma(Q)}{d\Omega} = \frac{C[f(Q)]^2}{N_{\rm cell}}\sum_{i,j}\sum_{a,b}\langle\mathbf{S}_{i\perp}^a\cdot\mathbf{S}_{j\perp}^b\rangle\mathrm{e}^{\imath\mathbf{Q}\cdot\mathbf{R}_{ij}^{ab}}, \qquad (11)$$

where $\mathbf{Q}$ is the momentum transfer, $\mathbf{Q}=\mathbf{G}+\mathbf{q}$, $\mathbf{G}$ is a reciprocal lattice vector and $\mathbf{q}$ is a vector in the first zone, $f(Q)$ is the magnetic form factor of the relevant scattering ion, and C is a constant. The spin-spin correlation function only involves spin components perpendicular to $\mathbf{Q}$ (i.e., $\mathbf{S}_{i\perp}^a=\mathbf{S}_i^a-(\mathbf{S}_i^a\cdot\mathbf{Q})\mathbf{Q}/|\mathbf{Q}|^2)$) and can be written as

$$\langle\mathbf{S}_{i\perp}^a\cdot\mathbf{S}_{j\perp}^b\rangle = \sum_{u,v}\left[\hat{n}^u\cdot\hat{n}^v-(\hat{n}^u\cdot\hat{Q})(\hat{n}^v\cdot\hat{Q})\right]\times\langle S_i^{a,u}S_j^{b,v}\rangle = \sum_{u,v}\left(\delta^{u,v}-\frac{Q^uQ^v}{|\mathbf{Q}|^2}\right)\langle S_i^{a,u}S_j^{b,v}\rangle, \qquad (12)$$

where $\hat{Q}=\mathbf{Q}/|\mathbf{Q}|$. The correlation function $\langle S_i^{a,u}S_j^{b,v}\rangle$ is expressed as a thermal average of the mean-field variables and then transformed to normal modes,

$$\langle S_i^{a,u} S_j^{b,v} \rangle = \sum_{\mathbf{q},\mathbf{q}'} \sum_{\alpha,\beta} \sum_{\mu,\nu} \langle \phi_{\mathbf{q}}^{\alpha,\mu} \phi_{\mathbf{q}'}^{\beta,\nu} \rangle U_{\mu,u}^{\alpha,a}(\mathbf{q}) U_{v,\nu}^{b,\beta}(\mathbf{q}') \times e^{-\imath \mathbf{q}\cdot\mathbf{R}_i^a} e^{-\imath \mathbf{q}'\cdot\mathbf{R}_j^b}. \quad (13)$$

The correlation function of normal mode variables is calculated from derivatives of the mean-field partition function, $Z=\mathrm{Tr}\{e^{-\beta \mathcal{F}_\rho(T)}\}$, where $\mathcal{F}_\rho(T)$ is given by Eq. (10), with respect to $\tilde{h}_{\mathbf{q}}^{\alpha,\mu}$. The result is

$$\langle \phi_{\mathbf{q}}^{\alpha,\mu} \phi_{\mathbf{q}'}^{\beta,\nu} \rangle = \frac{\delta^{\alpha,\beta}\delta^{\mu,\nu}\delta_{\mathbf{q}+\mathbf{q}',0}}{(3-\lambda^{\alpha,\mu}(\mathbf{q})/T)} \quad (14)$$

for Heisenberg spins and

$$\langle \phi_{\mathbf{q}}^{\alpha} \phi_{\mathbf{q}'}^{\beta} \rangle = \frac{\delta^{\alpha,\beta}\delta_{\mathbf{q}+\mathbf{q}',0}}{(1-\lambda^{\alpha}(\mathbf{q})/T)} \quad (15)$$

for $\langle 111 \rangle$ Ising spins.

Using Eqs. (12)–(14) or (15) in Eq. (11) and carrying out the sums, one obtains equations for the scattering cross section. In the case of Heisenberg spins, we have

$$\frac{1}{N_{\mathrm{cell}}} \frac{d\sigma(Q)}{d\Omega} = C[f(Q)]^2 \sum_{\alpha,\mu} \frac{|\mathbf{F}_{\mu,\perp}^{\alpha}(\mathbf{q})|^2}{(3-\lambda_{\mu}^{\alpha}(\mathbf{q})/T)}, \quad (16)$$

where

$$\mathbf{F}_{\mu,\perp}^{\alpha}(\mathbf{q}) = \sum_a \{\mathbf{U}_{\mu}^{\alpha,a}(\mathbf{q}) - (\mathbf{U}_{\mu}^{\alpha,a}(\mathbf{q})\cdot\hat{Q})\hat{Q}\} e^{\imath \mathbf{G}\cdot\mathbf{r}^a} \quad (17)$$

is a three-component vector. For $\langle 111 \rangle$ Ising spins, one has

$$\frac{1}{N_{\mathrm{cell}}} \frac{d\sigma(Q)}{d\Omega} = C[f(Q)]^2 \sum_{\alpha} \frac{|\mathbf{F}_{\perp}^{\alpha}(\mathbf{q})|^2}{(1-\lambda^{\alpha}(\mathbf{q})/T)}, \quad (18)$$

with

$$\mathbf{F}_{\perp}^{\alpha}(\mathbf{q}) = \sum_a \hat{z}_{\perp}^a U^{\alpha,a}(\mathbf{q}) e^{\imath \mathbf{G}\cdot\mathbf{r}^a}, \quad (19)$$

where $\mathbf{F}_{\perp}^{\alpha}(\mathbf{q})$ is still a three-component vector and $\hat{z}_{\perp}^a = \hat{z}^a - (\hat{z}^a\cdot\hat{Q})\hat{Q}$.

Equations (16) and (18) are the main results of this section. They provide a mean-field description for the PM elastic neutron scattering of Heisenberg and $\langle 111 \rangle$ Ising moments, respectively, on the pyrochlore lattice. The temperature that defines the paramagnetic regime is set by the maximum eigenvalue according to

$$T > T_c^{\mathrm{MF}} \equiv \max_{\mathbf{q}}\{\lambda^{\max}(\mathbf{q})\}/n, \quad (20)$$

where $\lambda^{\max}(\mathbf{q})$ is the maximum eigenvalue at wave vector $\mathbf{q}$, and $\max_{\mathbf{q}}$ selects the global maximum for all $\mathbf{q}$. The $\max_{\mathbf{q}}\{\lambda^{\max}(\mathbf{q})\}$ occurs at the ordering wave vector $\mathbf{q}_{\mathrm{ord}}$.

III. NEUTRON SCATTERING OF $Tb_2Ti_2O_7$

Starting with the zeroth-order (low-energy) $\langle 111 \rangle$ description for $Tb_2Ti_2O_7$, we use $J_1=-2.64$ K and $D=0.48$ K yielding $J_{\mathrm{nn}}/D_{\mathrm{nn}}=-1.1$ (Ref. 25), which compares to $J_{\mathrm{nn}}/D_{\mathrm{nn}}=-0.22$ for $Ho_2Ti_2O_7$ (Ref. 32) and $J_{\mathrm{nn}}/D_{\mathrm{nn}}=-0.52$ for $Dy_2Ti_2O_7$ (Ref. 35). Therefore, at a nearest-neighbor cutoff distance, $Tb_2Ti_2O_7$ is an AFM $\langle 111 \rangle$ pyrochlore that is predicted to develop noncollinear AFM order, with ordering wave vector $\mathbf{q}_{\mathrm{ord}}=\mathbf{0}$, at $T\approx 1$ K (Refs. 25 and 35). We emphasize that in the context of a $\langle 111 \rangle$ Ising model with $J_{\mathrm{nn}}/D_{\mathrm{nn}}=-1.1$, $Tb_2Ti_2O_7$ is still predicted to be a long-range AFM when both antiferromagnetic nearest-neighbor exchange and long-range dipole interactions are considered.[35] Hence, the antiferromagnetic exchange in a $\langle 111 \rangle$ model of $Tb_2Ti_2O_7$ is sufficiently strong to prevent the perturbations arising from long-range dipolar interactions from changing the ordered state of the model. The counterpoint to the above model predictions is that experimentally $Tb_2Ti_2O_7$ remains a collective paramagnetic down to very low temperatures, $T \gtrsim 50$ mK (Ref. 16).

As an initial attempt to explain the physics of $Tb_2Ti_2O_7$, we investigate the PM correlations within MFT and compare to the experimental results for elastic neutron scattering. Experimental data for elastic neutron scattering in $Tb_2Ti_2O_7$ are shown in Fig. 2(a). The most intense region of scattering is centered around $\mathbf{Q}=0,0,2$ with reduced correlations extending toward $\mathbf{Q}=2,2,0$ and a scattering minimum at $\mathrm{Q}=\mathbf{0}$. From the pyrochlore lattice structure and the MF formalism, we know that the intensity at $\mathbf{Q}=0,0,2$ is controlled by the eigenmodes at $\mathbf{Q}=0,0,0$ but modulated by the phase factor $\exp(\imath\mathbf{G}\cdot\mathbf{r}^a)$, see Eqs. (18) and (19). This raises the question as to whether the maximum about $\mathbf{Q}=0,0,2$ could be interpreted as the precursor of a long-range ordered noncollinear AFM state.

We begin by considering $\langle 111 \rangle$ Ising spins on the pyrochlore lattice. (The details upon which our arguments are based are provided in Appendix D.) The neutron-scattering intensity profile is determined by $\mathbf{F}_{\perp}^{\alpha}(\mathbf{q})$, Eq. (19), and contains information on the spin anisotropy via $\hat{z}^a$ and the eigenvalues $\lambda^{\alpha}(\mathbf{q})$ and the symmetry of the lattice through the eigenvectors $U^{\alpha,a}(\mathbf{q})$, and a phase factor $\exp(\imath\mathbf{G}\cdot\mathbf{r}^a)$. Hence, the nature and strength of the exchange and dipole-dipole interactions are arbitrary. From these basic symmetry components, we find that $|\mathbf{F}_{\perp}^{\alpha}(0,0,0)|^2=|\mathbf{F}_{\perp}^{\alpha}(0,0,2)|^2$ or that the scattering intensity about $\mathbf{Q}=0,0,0$ and $\mathbf{Q}=0,0,2$ has the same numerical value, disregarding the form factor $(f(Q))$. An equivalent statement is the intensities about $\mathbf{Q}=0,0,0$ and $\mathbf{Q}=0,0,2$ are symmetry related. This strong condition on the scattering pattern is in serious contradiction with the experimentally observed results. In contrast, if we consider an anisotropic Heisenberg pyrochlore model [Eq. (16) with finite Δ], we find that the lattice and spin degrees of freedom do not force the scattering intensity to be identical about $\mathbf{Q}=0,0,0$ and $\mathbf{Q}=0,0,2$. For a model with full $O(3)$ spin symmetry, the scattering profile is controlled by $\mathbf{F}_{\mu,\perp}^{\alpha}(\mathbf{q})$, Eq. (17). The significant difference between Eqs. (17) and (19) is the restoration of spin isotropy, i.e., the geometric factor defining the local $\langle 111 \rangle$ quantization axis $\hat{z}^a$ is absent from Eq. (17). Therefore, on purely symmetry grounds, no $\langle 111 \rangle$ Ising model (i.e., Hamiltonian) with arbitrary distance-dependent $J_{ij}(\mathbf{r_{ij}})$ for $Tb_2Ti_2O_7$ will reproduce the experimental PM correlations shown in Fig. 2(a). Earlier works have recognized the need to consider more isotropic spin models for $Tb_2Ti_2O_7$. In Ref. 41, the qualitative features of the PM scat-

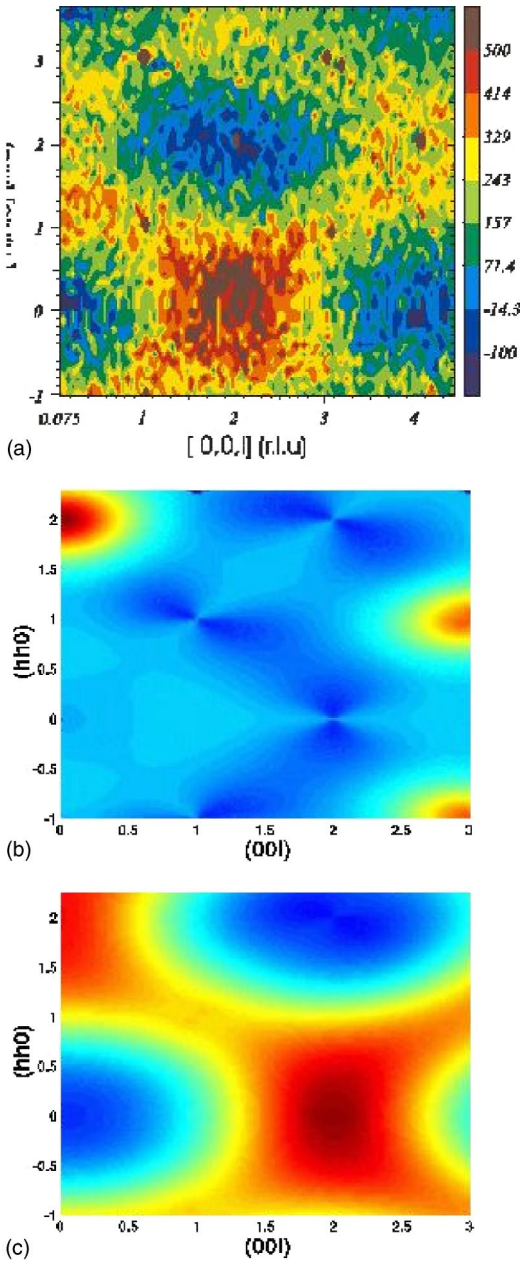

FIG. 2. (Color online) Paramagnetic scattering in the (*hhl*) plane for $Tb_2Ti_2O_7$: (a) Experimental paramagnetic scattering[41] ($T=9$ K), maximum intensity at $\mathbf{Q}=0,0,2$, (b) MF model of $Tb_2Ti_2O_7$ treated as a $\langle 111\rangle$ Ising pyrochlore ($T=1.5T_c^{\mathrm{MF}}$), no intensity at $\mathbf{Q}=0,0,2$, (c) MF model of $Tb_2Ti_2O_7$ treated as an anisotropic Heisenberg pyrochlore ($T=1.5T_c^{\mathrm{MF}}, \Delta=20$ K), maximum intensity at $\mathbf{Q}=0,0,2$.

tering were reproduced from an isotropic structure factor for the nearest-neighbor Heisenberg pyrochlore AFM. Similar results were obtained in Ref. 42 by considering specific $\mathbf{Q}=\mathbf{0}$ spin structures on a cluster of two tetrahedra.

To support the picture obtained on symmetry grounds, we have applied our MF formalism to two models for $Tb_2Ti_2O_7$: (i) a pyrochlore system with $\langle 111\rangle$ Ising spins, and (ii) a pyrochlore lattice with Heisenberg spins and finite $\langle 111\rangle$ anisotropy. In both cases, the dipole-dipole interactions are

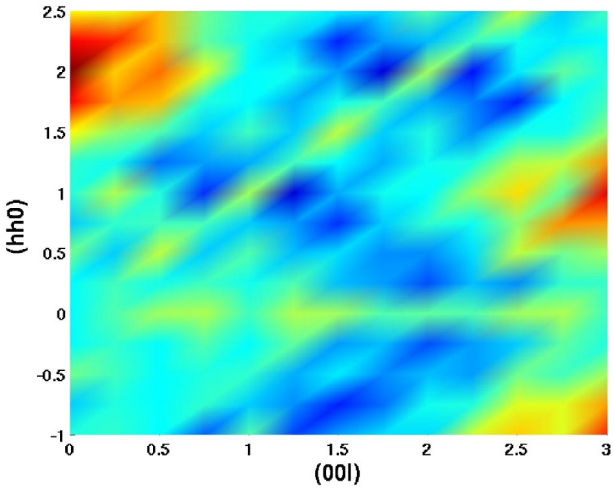

FIG. 3. (Color online) Monte Carlo results for paramagnetic scattering in the (*hhl*) plane for $Tb_2Ti_2O_7$ as a $\langle 111\rangle$ Ising AFM, $T=5.0$ K, $N=1024$ spins. Note that there is no intensity about $\mathbf{Q}=0,0,2$. Dipoles were treated via the Ewald method.

evaluated with the Ewald method, see Appendix C. For the $\langle 111\rangle$ Ising description [i.e., $\Delta/|J|\gg 1$ and $\Delta/D\gg 1$ and Eq. (18)], we use $J_1=-2.64$ K and $D=0.48$ K (Ref. 25). Our data are shown in Fig. 2(b). Note that the scattering about $\mathbf{Q}=0,0,0$ and $\mathbf{Q}=0,0,2$ is symmetry related, as predicted above, but is an intensity minimum. Monte Carlo data for this $\langle 111\rangle$ Ising model agrees with our MF results, see Fig. 3. Monte Carlo simulations for $Tb_2Ti_2O_7$ as a $\langle 111\rangle$ Ising dipolar model were performed on a $L=4$ lattice ($N=1024$ spins) at $T=5$ K ($T_c^{\mathrm{MF}}\sim 1$ K) with $J_1=-2.64$ K and $D=0.48$ K, with the dipolar sum treated via the Ewald summation method. Neutron-scattering data [as determined by Eq. (11) (Ref. 32)] were collected after 5×10^7 Monte Carlo steps per spin for both equilibration and measurement stages, and are shown in Fig. 3. The intensity minimum at $\mathbf{Q}=0,0,0$ and $\mathbf{Q}=0,0,2$ supports the above mean-field results and symmetry arguments. For a Heisenberg model with finite anisotropy [i.e., $\Delta/|J|>1$ and $\Delta/D>1$ and Eq. (16)], our MF results are provided in Fig. 2(c). With an anisotropy strength of $\Delta=20$ K (i.e., $\Delta/D\approx 41.7$), we achieve good qualitative agreement with the experiment. The region around $\mathbf{Q}=0,0,2$ has the strongest scattering with reduced intensity near $\mathbf{Q}=2,2,0$ and the interconnecting regions. If we turn off the finite anisotropy ($\Delta=0$), i.e., an isotropic Heisenberg model with long-range dipoles, the dominating scattering remains about points $\mathbf{Q}=0,0,2$ and $\mathbf{Q}=2,2,0$, but there is increased intensity along the bridge regions in $\mathbf{q}$-space connecting these points. Finally, in the absence of dipoles and $\Delta=0$ one has the nearest neighbor AFM exchange Heisenberg model, where the scattering intensity forms a network of interconnected triangles with equal intensity about $\mathbf{Q}=0,0,2$ and $\mathbf{Q}=2,2,0$ (Refs. 41, 64, and 65). Hence, a partial restoration of the spin isotropy is sufficient to place scattering about points $\mathbf{Q}=0,0,2$ and $\mathbf{Q}=2,2,0$ in $\mathbf{q}$-space, but to achieve good qualitative agreement with the experimental intensity profile dipolar interactions are necessary as is a finite single-ion contribution to the Hamiltonian.

IV. DISCUSSION

A. $Tb_2Ti_2O_7$

The prediction of an ⟨111⟩ Ising model for $Tb_2Ti_2O_7$ is that of an AFM long-range ordered state in which all spins point either in or out of the unit tetrahedra at $T \approx 10^0$ K. However, this prediction is not realized experimentally. Another problem, and possibly even more important, with a ⟨111⟩ Ising model for $Tb_2Ti_2O_7$, is that the mean-field PM correlations [see Fig. 2(b)] do not agree with the experimentally observed results [Fig. 2(a)]. In Section III and in Appendix D, we demonstrated on symmetry grounds alone that no pyrochlore model with ⟨111⟩ Ising moments could reproduce the basic features of the experimental PM scattering (i.e., strongest intensity centered about $\mathbf{Q}=0, 0, 2$, lower intensity about $\mathbf{Q}=2, 2, 0$, and minimum intensity at the zone center $\mathbf{Q}=0, 0, 0$). These symmetry arguments were also supported by MF and MC calculations of the elastic neutron-scattering cross section, Eq. (18).

In Section III and in Appendix D, we were also able to demonstrate on symmetry grounds that a Heisenberg pyrochlore model of $Tb_2Ti_2O_7$ would allow for elastic scattering about $\mathbf{Q}=0, 0, 2$ while at the same time permit no scattering about $\mathbf{Q}=0, 0, 0$. A MF calculation of the PM neutron scattering in the (hhl) plane for an anisotropic Heisenberg model with long-range dipoles, Eq. (1), shows good agreement with the experimental scattering pattern [strongest intensity about $\mathbf{Q}=0, 0, 2$ with reduced scattering at $\mathbf{Q}=2, 2, 0$ and along the bridges between these points, see Fig. 2(c)]. Both the finite anisotropy ($\Delta/|J|>1$ and $\Delta/D>1$) and long-range dipoles are necessary to achieve a quantitative match with the experiments. Reducing either the single-ion anisotropy to the isotropic limit ($\Delta=0$) or the range of the dipole-dipole interactions in the model reduces this agreement by altering the ratio of scattering intensity between $\mathbf{Q}=0, 0, 2$ and $\mathbf{Q}=2, 2, 0$. However, even a dramatically simplified model, which would have dipoles cut off at the first nearest neighbor $r_c=1$, would still improve the picture provided by a nearest-neighbor AFM exchange-only Heisenberg model presented in Ref. 41. Therefore, and foremost in our argument, a restoration of the spin isotropy is absolutely necessary to place paramagnetic scattering about the $\mathbf{q}$-space points $\mathbf{Q}=0, 0, 2$ and $\mathbf{Q}=2, 2, 0$. The dipolar interactions are then important for shifting (i.e., redistributing) the scattering intensity from $\mathbf{Q}=2, 2, 0$ to $\mathbf{Q}=0, 0, 2$. Intermediate regions between these two points also experience a reduction in scattering. In terms of the underlying soft-mode spectrum, the $\mathbf{q}=\mathbf{0}$ eigenvalues and eigenvectors control the scattering at $\mathbf{Q}=2, 2, 0$ to $\mathbf{Q}=0, 0, 2$. A shift in intensity from $\mathbf{Q}=2, 2, 0$ to $\mathbf{Q}=0, 0, 2$ signals a PM spin structure that prefers to lie in xy plane (i.e., neutron scattering at $\mathbf{Q}=0, 0, 2$ comes from spins with components perpendicular to this direction).

Switching to a model with fully isotropic Heisenberg spins (as in Ref. 41) restores all the spin symmetry in the paramagnetic limit. This picture is dramatically inconsistent with the experimentally determined single-ion structure of Tb^{3+} ($J=6$, $^7F_6$) in $Tb_2Ti_2O_7$, where a ground-state doublet is separated from the first excited doublet by an anisotropy gap of 20 K, close to the θ_{CW} temperature.[24,25] Therefore, a restoration of the full spin symmetry at $T<20$ K seems an unlikely explanation for the PM scattering at 9 K.

The current MF approach does not allow the single-ion properties to be systematically considered, but a RPA calculation does.[66] By retaining only the simplest energy-level structure in the Tb^{3+} wave function, the ground-state doublet and the first excited-state doublet, one can relax the strict ⟨111⟩ Ising constraint on the spins in a controlled approximation. Within the RPA, fluctuations out of the ground-state and into the first excited-state levels are equivalent to a fluctuating canting of spins away from the Ising geometry. In this case, the lowest-order fluctuations from the strict ⟨111⟩ Ising limit yield qualitative agreement with experiment for the paramagnetic spin-spin correlations.[66] Others have also proposed a simple relaxation scheme of the strict ⟨111⟩ Ising directions.[42] Theoretical work remains to be done to explain the failure of $Tb_2Ti_2O_7$ to order at a temperature of 1 K, and why it remains paramagnetic down to 50 mK (Refs. 15 and 41).

B. General discussion: Avenues for other studies

We now briefly discuss some puzzling experimental results for a few highly frustrated magnets. We note that the present mean-field formulation for the structure factor $S(\mathbf{q})$ could provide valuable insight on the development of magnetic correlations out of the PM regime for each of these systems. The first, very paradoxical, system is the antiferromagnetic $Gd_3Ga_5O_{12}$ garnet (GGG). This material, where Gd^{3+} is the magnetic ion with a spin $S=7/2$, consists of two sublattices of intertwined spirals of corner-sharing triangles. For classical Heisenberg spins coupled by nearest-neighbor antiferromagnetic exchange, each spiral on a garnet lattice structure should display a thermally induced spin-nematic order-by-disorder transition according to work by Moessner and Chalker.[64] Some precursors of spin coplanarity in GGG may have recently been observed in Mössbauer experiments.[49] In GGG, however, dipolar interactions are approximately 50% of the strength of the exchange interactions for nearest neighbors and is, consequently, a sizable perturbation to contend with in this system.[44] In zero-applied magnetic field, specific heat, magnetic susceptibility, and nonlinear susceptibility measurements on GGG strongly suggest that this material undergoes a spin-glass transition around 140 mK (Refs. 45 and 46). However, the nonlinear susceptibility χ_{nl} measurements indicate that the spin-glass transition in this material is unusual in that χ_{nl} exhibits two maxima.[46] In contrast to bulk measurements,[45,46] neutron-scattering experiments on powder samples of isotopically enriched ^{160}Gd (natural Gd has a huge neutron absorption cross section) indicates the development of spin-spin correlations at approximatively 140 mK, extending to a length scale of ~100 Å(Refs. 47 and 48). It is unclear at present whether or not the development of extended spin correlations in GGG at ~140 mK is an intrinsic effect or is due to material impurities and/or defects (e.g., Gd^{3+} magnetic ions at Ga^{3+} sites[67]). Another interesting system is the $Gd_2Ti_2O_7$ pyrochlore antiferromagnet, where there, too, Gd^{3+} is the moment-carrying species. In $Gd_2Ti_2O_7$, the dipolar interactions are approxi-

mately 20% of the strength of the exchange interactions for nearest neighbors and is here, just as in GGG above, an important perturbation.[4,5,50] Palmer and Chalker argue that the ground state consists of a fully ordered structure where each tetrahedral unit cell has an identical (zero total magnetic moment) spin configuration (a so-called $\mathbf{q}_{\mathrm{ord}}=\mathbf{0}$ structure).[5] Recent work has confirmed that this ground state is extremely robust against quantum fluctuations.[53] However, recent experiments on $Gd_2Ti_2O_7$ are rather puzzling and appear inconsistent with Palmer and Chalker's work. Specifically, neutron diffraction measurements on ^{160}Gd isotopically enriched powders find a partially ordered phase with one disordered sublattice and propagation vector $\mathbf{q}=\frac{1}{2},\frac{1}{2},\frac{1}{2}$ at $T=50$ mK,[6] hence incompatible with the predictions of Palmer and Chalker.[5] Specific heat measurements find strong evidence for two transitions at $T=0.7$ K and at $T=1.0$ K (Ref. 50). Recent mean-field calculations find evidence for a two-step magnetic ordering in this system.[68,69] So for $Gd_2Ti_2O_7$, there also exists a complex behavior as signaled by thermodynamic measurements, theoretical predictions, and neutron-scattering results.[70] Finally, the $Yb_2Ti_2O_7$ pyrochlore ferromagnet is also puzzling.[26,52] There, neutron-scattering results, muon spin relaxation, and Mössbauer experiments suggest a ground state that lacks long-range magnetic order while there exist good evidence from the Mössbauer data that a first-order spin-freezing transition occurs around $T_f\sim 0.24$ K. Meanwhile, elastic neutron-scattering results reveal the development of nontrivial spin-spin correlations as T_f is approached from above. In this system too, it is possible that long-range dipolar interactions may play some role due to the contribution of the $|J,m_J\rangle=|7/2,\pm 7/2\rangle$ eigenstate within the effective $S_{\mathrm{eff}}=1/2$ ground-state doublet.[26]

V. CONCLUSIONS

In conclusion, we have demonstrated on symmetry grounds, through MF calculations, and MC simulations that the experimentally measured PM elastic neutron scattering in $Tb_2Ti_2O_7$ is inconsistent with a $\langle 111\rangle$ Ising pyrochlore spin structure. From the qualitative agreement obtained using an anisotropic Heisenberg model, we argue in favor of a more isotropic effective spin model to describe the low-energy phases of $Tb_2Ti_2O_7$.

Finally, we have discussed the usefulness of a combined mean-field theory and Ewald method approach to studying geometrically frustrated magnets with long-range dipole-dipole interactions in the paramagnetic phase. This approach could be applied in general to any geometrically frustrated system. The zero field picture of $Gd_3Ga_5O_{12}$ (GGG) is particularly interesting because the low-temperature phase remains an unresolved issue that entails unraveling the physics of competing exchange and long-range dipole-dipole interactions in a garnet lattice environment.[45–49,71]

ACKNOWLEDGMENTS

We would like to acknowledge Bill Buyers, Steve Bramwell, Adrian del Maestro, Jason Gardner, Bruce Gaulin, Byron den Hertog, Ying-Jer Kao, Jean-Yves Delannoy, Roger Melko, Adrian del Maestro, Hamid Molavian, and Taras Yavors'kii for many useful discussions. This work is supported by NSERC of Canada, the Canada Research Chairs Program, Research Corporation, and the Province of Ontario.

APPENDIX A: NEUTRON SCATTERING IN THE GAUSSIAN APPROXIMATION

As we noted in the Introduction, other authors have discussed MFT and its application to magnetism[39,54–57] and the Ewald method for magnetic dipoles.[59–61] Our purpose is to combine the techniques of MFT, developed here, with the Ewald procedures for magnetic dipoles in $\mathbf{q}$-space (developed in Appendix C so they can be readily applied to other problems of highly frustrated rare-earth magnets.

In this appendix we provide a detailed derivation of the mean-field equations for the elastic-scattering cross section for pyrochlore spin systems. Our derivation is performed for Heisenberg spins, with a finite local $\langle 111\rangle$ anisotropy, in order to broaden the appeal of the results. Connections to $\langle 111\rangle$ Ising systems, infinite local $\langle 111\rangle$ anisotropy, are noted at appropriate points. As mentioned in Section II, the MFT is developed via a variational approach (VMFT) and, in general, this approach applies to a large array of statistical models with arbitrarily complex order parameters.[54] In this work, the method reproduces the Gaussian approximation (GA) of the Landau free energy. The VMFT described here has been used by others,[39,55–57] and we provide a detailed presentation here to clear up the notational inconsistencies that appeared in some of these previous works. We also wish to provide for comparison with the RPA, which allows for a more controlled relaxation of the $\langle 111\rangle$ Ising restriction[62,66] that experimental evidence suggests is needed for $Tb_2Ti_2O_7$[41,42]

We begin with the model Hamiltonian of Eq. (1), H_H. The conventions for the spin vectors $\mathbf{S}_i^a$, unit vectors $\hat{n}^u$, and $\hat{z}^a$, and the description of the pyrochlore lattice in a rhombohedral basis with a four-atom unit cell are as described in Section II. Therefore, our starting Hamiltonian for MFT is given by

$$H_H=-\frac{1}{2}\sum_{i,j}\sum_{a,b}\sum_{u,v}\mathcal{J}_{uv}^{ab}(i,j)S_i^{a,u}S_j^{b,v}-\sum_{i,a,u}h_i^{a,u}S_i^{a,u}, \quad \text{(A1)}$$

where $\mathcal{J}_{uv}^{ab}(i,j)$ is defined by Eq. (5), and a fictitious field term has been added. The field term, with $|\mathbf{h}_i^a|=|\mathbf{h}|$, is removed from the final equations by taking $\mathbf{h}_i^a\rightarrow 0$. We note that indices $(a,b)=1$, 2, 3, 4 label the sublattices and $(u,v)=1$, 2, 3 label the spin components.

In VMFT, an approximate free energy as a function of a trial density matrix ρ is formed,

$$F_\rho=\mathrm{Tr}\{\rho H_H\}+T\,\mathrm{Tr}\{\rho\ln\rho\}=\langle H_H\rangle_\rho+T\langle\ln\rho\rangle_\rho, \quad \text{(A2)}$$

where Tr represents a trace-over spin variables. F_ρ is variational and defines an upper bound to the actual free energy, i.e., $F_\rho\geqslant F$. The best functional from for the trial density matrix is obtained by minimizing F_ρ with respect to the parameters of ρ. For a system of N particles, the MF form of the N-body density matrix is given by a product of single particle density matrices,

$$\rho(\{\mathbf{S}_i^a\}) = \prod_{i,a} \rho_i^a(\mathbf{S}_i^a). \tag{A3}$$

The single particle density matrix ρ_i^a is treated as a variational parameter that is subject to the constraints

$$\mathrm{Tr}\{\rho_i^a\} = 1, \tag{A4}$$

$$\mathrm{Tr}\{\rho_i^a \mathbf{S}_i^a\} = \mathbf{m}_i^a, \tag{A5}$$

which keep the internal energy constant, i.e., $\mathrm{Tr}\{\rho H\} = C$. Here, $\mathbf{m}_i^a$ is a vector-order parameter; for $\langle 111\rangle$ Ising spins, one has the scalar equivalent, $\mathrm{Tr}\{\rho_i^a \sigma_i^a\} = m_i^a$. Incorporating the constraints into the expression for F_ρ gives

$$F_\rho = \mathrm{Tr}\{\rho H_H\} + T\,\mathrm{Tr}\{\rho \ln \rho\} - T\,\mathrm{Tr}\left\{\sum_{i,a} \xi_i^a(\rho_i^a - 1)\right\} - T\,\mathrm{Tr}\left\{\sum_{i,a} (\rho_i^a \mathbf{S}_i^a - \mathbf{m}_i^a)\cdot \mathbf{A}_i^a\right\}, \tag{A6}$$

where ξ_i^a and $\mathbf{A}_i^a$ are the Lagrange multipliers for the constraints of Eq. (A4) and Eq. (A5), respectively. In minimizing F_ρ with respect to ρ_i^a, one has the following results:

$$\frac{\delta}{\delta \rho_i^a}\,\mathrm{Tr}\{\rho H_H\} = 0,$$

$$\frac{\delta}{\delta \rho_i^a}\,\mathrm{Tr}\{\rho \ln \rho\} = \mathrm{Tr}\{\ln \rho_i^a\} + \mathrm{Tr}\{1\},$$

$$\frac{\delta}{\delta \rho_i^a}\,\mathrm{Tr}\left\{\sum_{i,a} \xi_i^a \rho_i^a\right\} = \mathrm{Tr}\{\xi_i^a\},$$

$$\frac{\delta}{\delta \rho_i^a} T\,\mathrm{Tr}\left\{\sum_{i,a} \rho_i^a \mathbf{S}_i^a \cdot \mathbf{A}_i^a\right\} = \mathrm{Tr}\{\mathbf{S}_i^a \cdot \mathbf{A}_i^a\}.$$

The optimum form for the density matrix is found by solving $\delta F_\rho / \delta \rho_i^a = 0$,

$$\rho_i^a = \mathcal{C}_i^a e^{\mathbf{A}_i^a \cdot \mathbf{S}_i^a}, \tag{A7}$$

where $\mathcal{C}_i^a = e^{\xi_i^a - 1} = 1/\mathrm{Tr}\{e^{A_i^a \cdot S_i^a}\}$ follows from Eq. (4). Evaluating the trace in $\mathcal{C}_i^a$ for both Heisenberg and Ising spins we obtain

$$\mathcal{Z}_i^a = \frac{(2\pi)^{3/2}}{(|\mathbf{A}_i^a|)^{1/2}} I_{1/2}(|\mathbf{A}_i^a|) = \frac{4\pi}{|\mathbf{A}_i^a|}\sinh(|\mathbf{A}_i^a|) \tag{A8}$$

and

$$\mathcal{Z}_i^a = 2\cosh(A_i^a), \tag{A9}$$

respectively, where $I_{1/2}(|\mathbf{A}_i^a|)$ is a modified Bessel function. The variational local density matrix is now written as

$$\rho_i^a = \frac{e^{\mathbf{A}_i^a \cdot \mathbf{S}_i^a}}{\mathcal{Z}_i^a} \tag{A10}$$

and is used, along with the constraints of Eqs. (A4) and (A5),to rewrite the variational free energy,

$$F_\rho = -\tfrac{1}{2}\sum_{i,j}\sum_{a,b}\sum_{u,v} \mathcal{J}_{uv}^{ab}(i,j) m_i^{a,u} m_j^{b,v} - \sum_{i,a,u} h_i^{a,u} m_i^{a,u} + T\sum_{i,a} (\mathbf{A}_i^a \cdot \mathbf{m}_i^a - \ln \mathcal{Z}_i^a). \tag{A11}$$

We want an expression for the free-energy–to–quadratic order in $\mathbf{m}_i^a$. This means that one must expand $\ln \mathcal{Z}_i^a(\mathbf{A}_i^a)$ and then express $\mathbf{A}_i^a$ as a function of $\mathbf{m}_i^a$. From the series representation of $\mathcal{Z}_i^a(\mathbf{A}_i^a)$ followed by the series expansion of $\ln(1-x)$, one has

$$\ln \mathcal{Z}_i^a \approx \ln C_1 + \frac{|\mathbf{A}_i^a|^2}{2n}, \tag{A12}$$

where C_1 is a model-dependent constant and $n = 1, 3$ for Ising and Heisenberg spins, respectively. Using Eq. (A5), one obtains the expression

$$m_i^a = \hat{A}_i^a \frac{I_{3/2}(|\mathbf{A}_i^a|^2)}{I_{1/2}(|\mathbf{A}_i^a|^2)} \tag{A13}$$

$$= \hat{A}_i^a \left\{ \mathrm{Coth}(|\mathbf{A}_i^a|) - \frac{1}{|\mathbf{A}_i^a|}\right\} \tag{A14}$$

for Heisenberg and

$$m_i^a = \tanh(A_i^a) \tag{A15}$$

for Ising spins. To first order, we have

$$\mathbf{m}_i^a = 3\mathbf{A}_i^a \tag{A16}$$

and

$$m_i^a = A_i^a. \tag{A17}$$

Using Eqs. (A12)–(A17), we can write the MF free energy to quadratic order in the order parameter,

$$F_\rho = \tfrac{1}{2}\sum_{i,j}\sum_{a,b}\sum_{u,v} m_i^{a,u}\{nT\delta_{i,j}\delta^{a,b}\delta^{u,v} - \mathcal{J}_{uv}^{ab}(i,j)\} m_j^{b,v} - \sum_{i,a,u} h_i^{a,u} m_i^{a,u} - TpN_{\mathrm{cell}} \ln C_1, \tag{A18}$$

where $p = 4$ denotes the size of the basis (sublattice). As a side note, the Lagrange multiplier $\mathbf{A}_i^a$ can be interpreted as an effective mean field interacting with a local moment. Minimizing F_ρ, of Eq. (A11) with respect to $m_i^{a,u}$ one has

$$A_i^{a,u} = \frac{\overline{h}_i^{a,u}}{T}, \tag{A19}$$

where

$$\overline{h}_i^{a,u} = \sum_{j,b,v} \mathcal{J}_{uv}^{ab}(i,j) m_j^{b,v} + h_i^{a,u}, \tag{A20}$$

is the uth component of the effective field at site (i,a). We next exploit the fact that the pyrochlore lattice has the underlying symmetry of a fcc lattice by defining the Fourier transforms,

$$m_i^{a,u} = \sum_{\mathbf{q}} m_{\mathbf{q}}^{a,u} e^{-\imath \mathbf{q}\cdot \mathbf{R}_i^a}, \tag{A21}$$

$$\mathcal{J}_{uv}^{ab}(i,j) = \frac{1}{N_{\text{cell}}} \sum_{\mathbf{q}} \mathcal{J}_{uv}^{ab}(\mathbf{q}) e^{\imath \mathbf{q}\cdot\mathbf{R}_{ij}^{ab}}, \tag{A22}$$

where N_{cell} is the number of fcc Bravais lattice points, but $\mathbf{R}_i^a$ denotes the position of a spin, and $\mathbf{R}_{ij}^{ab} = \mathbf{R}_i^a - \mathbf{R}_j^b$. Equations (A21) and (A22) applied to F_ρ yield

$$\mathcal{F}_\rho(T) = \tfrac{1}{2} \sum_{\mathbf{q}} \sum_{a,b} \sum_{u,v} m_{\mathbf{q}}^{a,u} [nT\delta^{a,b}\delta^{u,v} - \mathcal{J}_{uv}^{ab}(\mathbf{q})] m_{-\mathbf{q}}^{b,v} - \sum_{\mathbf{q}} \sum_{a,b} \sum_{u,v} \delta^{a,b}\delta^{u,v} h_{\mathbf{q}}^{a,u} m_{-\mathbf{q}}^{b,v} - Tp \ln C_1, \tag{A23}$$

where $\mathcal{F}_\rho(T) = F_\rho(T)/N_{\text{cell}}$. A transformation to normal modes is necessary to diagonalize $\mathcal{J}_{uv}^{ab}(\mathbf{q})$. This is accomplished by the use of Eq. (9), or

$$m_{\mathbf{q}}^{a,u} = \sum_{\alpha=1}^{4} \sum_{\mu=1}^{3} U_{u,\mu}^{a,\alpha}(\mathbf{q}) \phi_{\mathbf{q}}^{\alpha,\mu}, \tag{A24}$$

where the Greek indices (α, μ) label the normal modes. $U(\mathbf{q})$ is the unitary matrix that diagonalizes $\mathcal{J}(\mathbf{q})$ in the sublattice space with eigenvalues $\lambda(\mathbf{q})$,

$$U^\dagger(\mathbf{q}) \mathcal{J}(\mathbf{q}) U(\mathbf{q}) = \lambda(\mathbf{q}), \tag{A25}$$

where in component form $U_{u,\mu}^{a,\alpha}(\mathbf{q})$ represents the (a,u) component of the (α,μ) eigenvector at $\mathbf{q}$ with eigenvalue $\lambda_\mu^\alpha(\mathbf{q})$. The amplitudes of the normal modes are denoted by $\{\phi_{\mathbf{q}}\} = \{\Sigma_{\alpha,\mu} \phi_{\mathbf{q}}^{\alpha,\mu}\}$. Therefore, the MF free-energy–to–quadratic order in the normal modes variables reads

$$\mathcal{F}_\rho(T) = \tfrac{1}{2} \sum_{\mathbf{q}} \sum_{\alpha,\mu} \phi_{\mathbf{q}}^{\alpha,\mu} [nT - \lambda_\mu^\alpha(\mathbf{q})] \phi_{-\mathbf{q}}^{\alpha,\mu} - T \sum_{\mathbf{q}} \sum_{\alpha,\mu} \tilde{h}_{\mathbf{q}}^{\alpha,\mu} \phi_{-\mathbf{q}}^{\alpha,\mu} - Tp \ln C_1, \tag{A26}$$

where

$$\tilde{h}_{\mathbf{q}}^{\alpha,\mu} = \frac{1}{T} \sum_{a,u} \mathbf{h}_{\mathbf{q}}^{a,u} U_{u,\mu}^{a,\alpha}(-\mathbf{q}).$$

Note that for the Ising case, the indices representing the spin components (u,v) and the corresponding modes (μ,ν) are dropped from Eq. (A26).

The neutron-scattering cross-section for unpolarized neutrons in the dipole approximation is given by Eq. (11) (Refs. 62 and 63, or

$$\frac{d\sigma(Q)}{d\Omega} = \frac{C[f(Q)]^2}{N_{\text{cell}}} \sum_{i,j} \sum_{a,b} \langle \mathbf{S}_{i\perp}^a \cdot \mathbf{S}_{j\perp}^b \rangle e^{\imath \mathbf{Q}\cdot\mathbf{R}_{ij}^{ab}}, \tag{A27}$$

where $\mathbf{Q}$ is the momentum transfer, i.e., $\mathbf{Q} = \mathbf{G} + \mathbf{q}$, $\mathbf{G}$ is a fcc reciprocal lattice vector, $\mathbf{q}$ is a wave vector in the first Brillouin zone, and C is a constant. The correlation function is between spin components perpendicular to the vector $\mathbf{Q}$,

$$\langle \mathbf{S}_{i\perp}^a \cdot \mathbf{S}_{j\perp}^b \rangle = \sum_{u,v} (\hat{n}_\perp^u \cdot \hat{n}_\perp^v) \langle S_i^{a,u} S_j^{b,v} \rangle = \sum_{u,v} \left(\delta^{u,v} - \frac{Q^u Q^v}{|\mathbf{Q}|^2} \right) \langle S_i^{a,u} S_j^{b,v} \rangle, \tag{A28}$$

where $\hat{n}_\perp^u = \hat{n}^u - (\hat{n}^u \cdot \hat{Q}) \hat{Q}$ is strictly a geometric factor and $\hat{Q} = \mathbf{Q}/|\mathbf{Q}|$. For Ising spins one replaces $\hat{n}^u$ with $\hat{z}^a$ from Table I and $S_i^{a,u}$ with σ_i^a. In order to proceed, the correlation function between spin variables, $\langle \mathbf{S}_{i\perp}^a \cdot \mathbf{S}_{j\perp}^b \rangle$, must be transformed to $\mathbf{q}$-space by use of Eq. (A21) and then to normal mode variables by application of Eq. (A24), one arrives at

$$\langle S_i^{a,u} S_j^{b,v} \rangle = \sum_{\mathbf{q},\mathbf{q}'} \sum_{\alpha,\beta} \sum_{\mu,\nu} \langle \phi_{\mathbf{q}}^{\alpha,\mu} \phi_{\mathbf{q}'}^{\beta,\nu} \rangle \times U_{\mu,u}^{\alpha,a}(\mathbf{q}) U_{v,\nu}^{b,\beta}(\mathbf{q}') e^{-\imath \mathbf{q}\cdot\mathbf{R}_i^a - \imath \mathbf{q}'\cdot\mathbf{R}_j^b}. \tag{A29}$$

The correlation function $\langle \phi_{\mathbf{q}}^{\alpha,\mu} \phi_{\mathbf{q}'}^{\beta,\nu} \rangle$ can be calculated from a partition function defined in terms of the normal mode amplitudes. The general definition reads

$$Z = \text{Tr}\{e^{-\mathcal{F}_\rho(T)/T}\}, \tag{A30}$$

where $\mathcal{F}_\rho(T)$ is given by Eq. (A26), and the trace is over all values of the normal mode amplitudes,

$$\text{Tr} \equiv \int_{-\infty}^{\infty} \prod_{\mathbf{q},\alpha,\mu} d\phi_{\mathbf{q}}^{\alpha,\mu},$$

so one has

$$Z = \prod_{\mathbf{q},\alpha,\mu} \int_{-\infty}^{\infty} d\phi_{\mathbf{q}}^{\alpha,\mu} e^{-\frac{1}{2}\left(n - \frac{\lambda_\mu^\alpha(\mathbf{q})}{T}\right) |\phi_{\mathbf{q}}^{\alpha,\mu}|^2 + \tilde{h}_{\mathbf{q}}^{\alpha,\mu} \phi_{-\mathbf{q}}^{\alpha,\mu}}, \tag{A31}$$

where a constant term has been dropped. The integral above is recast as a general Gaussian,

$$\int_{-\infty}^{\infty} d\phi e^{-\frac{1}{2}A\phi^2 + B\phi} = \sqrt{\frac{2\pi}{A}} e^{\frac{B^2}{2A}}, \tag{A32}$$

where $A = (n - [\lambda_\mu^\alpha(\mathbf{q})]/T)$ and $B = \tilde{h}_{\mathbf{q}}^{\alpha,\mu}$. Therefore, the final form of the partition function is

$$Z = \prod_{\mathbf{q},\alpha,\mu} Z^{\alpha,\mu}(\mathbf{q}) = \prod_{\mathbf{q},\alpha,\mu} \left[\frac{2\pi}{n - \frac{\lambda_\mu^\alpha(\mathbf{q})}{T}} \right]^{(1/2)} e^{|\tilde{h}_{\mathbf{q}}^{\alpha,\mu}|^2 / 2[n - \lambda_\mu^\alpha(\mathbf{q})/T]}. \tag{A33}$$

The correlation function is now determined from derivatives of Z with respect to the fields $\tilde{h}_{\mathbf{q}}^{\alpha,\mu}$,

$$\langle \phi_{\mathbf{q}}^{\alpha,\mu} \phi_{\mathbf{q}'}^{\beta,\nu} \rangle = \frac{1}{Z} \left| \frac{\partial^2 Z}{\partial \tilde{h}_{\mathbf{q}}^{\alpha,\mu} \partial \tilde{h}_{\mathbf{q}'}^{\beta,\nu}} \right|_{\tilde{h}_q = 0} = \frac{\delta_{\mathbf{q}+\mathbf{q}',0} \delta^{\alpha,\beta} \delta^{\mu,\nu}}{\left(n - \frac{\lambda_\mu^\alpha(\mathbf{q})}{T} \right)}. \tag{A34}$$

Back substitution of the result from Eq. (A34), into Eq. (A29), (A28), and then into Eq. (A27), and finally imposing the properties of the Kronecker delta functions leaves

$$\frac{1}{N_{\text{cell}}} \frac{d\sigma(Q)}{d\Omega} = C[f(Q)]^2 \sum_{\alpha,\mu} \sum_{a,b} \sum_{u,v} \frac{(\hat{n}_\perp^u \cdot \hat{n}_\perp^v)}{(n - \lambda_\mu^\alpha(\mathbf{q})/T)} \times U_{\mu,u}^{\alpha,a}(\mathbf{q}) U_{v,\mu}^{b,\alpha}(-\mathbf{q}) e^{\imath \mathbf{G}\cdot\mathbf{r}^{ab}}, \tag{A35}$$

where we have used the identity

$$\sum_{i,j} e^{\imath(\mathbf{Q}-\mathbf{q})\cdot\mathbf{R}_{ij}} e^{\imath(\mathbf{Q}-\mathbf{q})\cdot\mathbf{r}^{ab}} = N_{\text{cell}}^2 e^{\imath\mathbf{G}\cdot\mathbf{r}^{ab}}.$$

We find it convenient to define the function,

$$\mathbf{F}^{\alpha}_{\mu,\perp}(\mathbf{q}) = \sum_{a,u} \hat{n}^u_{\perp} U^{\alpha,a}_{\mu,u}(\mathbf{q}) e^{\imath\mathbf{G}\cdot\mathbf{r}^a}$$

$$= \sum_{a} \{\mathbf{U}^{\alpha,a}_{\mu}(\mathbf{q}) - [\mathbf{U}^{\alpha,a}_{\mu}(\mathbf{q})\cdot\hat{Q}]\hat{Q}\} e^{\imath\mathbf{G}\cdot\mathbf{r}^a}, \quad \text{(A36)}$$

where $\mathbf{U}^{\alpha,a}_{\mu}(\mathbf{q}) = \Sigma_u \hat{n}^u U^{\alpha,a}_{\mu,u}(\mathbf{q})$ [and, therefore, $\mathbf{F}^{\alpha}_{\mu,\perp}(\mathbf{q})$] is a three-component vector. The scattering cross section is written compactly as

$$\frac{1}{N_{\text{cell}}}\frac{d\sigma(Q)}{d\Omega} = C[f(Q)]^2 \sum_{\alpha,\mu} \frac{|\mathbf{F}^{\alpha}_{\mu,\perp}(\mathbf{q})|^2}{(n - \lambda^{\alpha}_{\mu}(\mathbf{q})/T)}, \quad \text{(A37)}$$

which is Eq. (16) with $n=3$. When considering $\langle 111\rangle$ Ising spins, the arguments that follow Eq. (A29) still hold, but the indices for the spin components (u,v) and corresponding normal modes (μ,ν) are dropped from the equations. The final expression for the scattering cross-section reads

$$\frac{1}{N_{\text{cell}}}\frac{d\sigma(Q)}{d\Omega} = C[f(Q)]^2 \sum_{\alpha} \frac{|\mathbf{F}^{\alpha}_{\perp}(\mathbf{q})|^2}{(1 - \lambda^{\alpha}(\mathbf{q})/T)}, \quad \text{(A38)}$$

where $\mathbf{F}^{\alpha}_{\perp}(\mathbf{q})$ is a three component vector given by

$$\mathbf{F}^{\alpha}_{\perp}(\mathbf{q}) = \sum_{a} \hat{z}^a_{\perp} U^{\alpha,a}(\mathbf{q}) e^{\imath\mathbf{G}\cdot\mathbf{r}^a}, \quad \text{(A39)}$$

which is just Eq. (18). We note that Eqs. (A37) and (A38) are only valid for $T > \lambda^{\alpha}_{\mu}(\mathbf{q}_{\text{ord}})/n$, where $\lambda^{\alpha}_{\mu}(\mathbf{q}_{\text{ord}}) = \max_{\mathbf{q}}\{\lambda^{\max}(\mathbf{q})\}$ is the critical eigenvalue, a global maximum, which sets T_c^{MF} and defines the paramagnetic regime. We also point out that the lattice structure and spin symmetry are contained in the respective $\mathbf{F}_{\perp}(\mathbf{q})$-functions, Eqs. (A36) and (A39); these properties will be exploited in Appendix D when we discuss symmetry-allowed scattering patterns for Heisenberg and Ising spins.

1. Comment on the convention for the Fourier transform

Another convention for defining Fourier modes uses the Bravais lattice points, $\mathbf{R}_i$, in the definitions,[72]

$$m^{a,u}_i = \sum_{\mathbf{q}} m^{a,u}_{\mathbf{q}} e^{-\imath\mathbf{q}\cdot\mathbf{R}_i}, \quad \text{(A40)}$$

and

$$\mathcal{J}^{ab}_{uv}(i,j) = \frac{1}{N_{\text{cell}}} \sum_{\mathbf{q}} \mathcal{J}^{ab}_{uv}(\mathbf{q}) e^{\imath\mathbf{q}\cdot\mathbf{R}_{ij}}. \quad \text{(A41)}$$

Hence, this convention differs from the one we employ by a simple phase factor, $\exp(\imath\mathbf{q}\cdot\mathbf{r}^{ab})$ for $\mathcal{J}^{ab}_{uv}(i,j)$. The two approaches are equally valid and yield the same results; however, there are a couple of important differences in the above results when this alternate convention is used. First, the interaction matrix defined by the inverse of Eq. (A41) has complex entries. For nearest-neighbor interactions between sites $a=1$ and $b=2$, we have

$$\mathcal{J}^{ab}_{uv}(\mathbf{q}) = \mathcal{J}^{1,2}_{uv}(1 + e^{-\imath\mathbf{q}\cdot\mathbf{R}_{i,j}}), \quad \text{(A42)}$$

where the factor of 1 arises because the sites $a=1$ and $b=2$ are in the same tetrahedral basis unit, i.e., $\mathbf{R}_{i,j}=\mathbf{0}$, but its symmetric equivalent has $\mathbf{R}_{i,j}\neq\mathbf{0}$. Next, the definition for the scattering cross section, Eq. (A27), holds, but the expression for the correlation function between normal-mode variables, Eq. (A29), contains the phase-factor $\exp(-\imath\mathbf{q}\cdot\mathbf{R}_i - \imath\mathbf{q}'\cdot\mathbf{R}_j)$. Carrying the necessary steps through to an expression for scattering cross section, one finds that the factor $\exp(\imath\mathbf{G}\cdot\mathbf{r}^a)$ in Eqs. (A36) and (A39) is replaced by $\exp(\imath\mathbf{Q}\cdot\mathbf{r}^a)$. Recall that momentum transfer and reciprocal lattice vector are related according to $\mathbf{Q}=\mathbf{G}+\mathbf{q}$. The presentation found in Refs. 39 and 56 (as noticed recently by Kadowaki *et al.*[73]) unintentionally mixes these two conventions.

APPENDIX B: HIGH TEMPERATURE EXPANSION OF THE GAUSSIAN APPROXIMATION

We demonstrate that the equations for the neutron-scattering cross section obtained from MFT at the Gaussian level (Appendix A) can also be formulated via a high-temperature series expansion (HTSE) to lowest order in $\beta \equiv 1/T$, where T is temperature in units of k_B. In contrast to VMFT, in a HTSE there is no appeal to any simplifying approximation that changes the character of the density matrix and imposes constraints that keep the internal energy $\text{Tr}\{\rho H\}$ fixed. We follow our established convention of treating the general case of anisotropic Heisenberg spins while pointing out the specific differences for $\langle 111\rangle$ Ising spins when needed. The starting point is the Heisenberg Hamiltonian of Eq. (1).

$$H_H = -\tfrac{1}{2}\sum_{i,j}\sum_{a,b}\sum_{u,v} \mathcal{J}^{ab}_{uv}(i,j) S^{a,u}_i S^{b,v}_j, \quad \text{(B1)}$$

where $\mathcal{J}^{ab}_{uv}(i,j)$ contains both spin and coordinate degrees of freedom and is defined by Eq. (5).

In the formula for the scattering cross section, Eq. (11), one must calculate the perpendicular correlation function,

$$\langle \mathbf{S}^a_{i\perp}\cdot\mathbf{S}^b_{j\perp}\rangle = \sum_{u,v} (\hat{n}^u_{\perp}\cdot\hat{n}^v_{\perp})\langle S^{a,u}_i S^{b,v}_j\rangle, \quad \text{(B2)}$$

which is just Eq. (12). We express the correlation function $\langle S^{a,u}_i S^{b,v}_j\rangle$ as a series expansion in cumulants,[74]

$$\langle S^{a,u}_i S^{b,v}_j\rangle = \sum_{m=0}^{\infty} \frac{(-\beta)^m}{m!}\langle S^{a,u}_i S^{b,v}_j H^m_H\rangle_c, \quad \text{(B3)}$$

where $\langle\ldots\rangle$ represents a thermal average with respect to H_H and $\langle\ldots\rangle_c$ represents the cumulant expansion of the spin operators and H_H. Cumulants are evaluated as a trace over the $T=0$ states, $\langle\ldots\rangle_0 = \text{Tr}\{\ldots\}/\text{Tr}\{1\}$, where $\text{Tr}\{1\}=\tilde{N}$ is a normalization factor, $(4\pi)^N$ for Heisenberg spins and $(2)^N$ for Ising spins, and N is the total number of sites in the lattice. Therefore, the correlation function to lowest order in β is

$$\langle S^{a,u}_i S^{b,v}_j\rangle \approx \langle S^{a,u}_i S^{b,v}_j\rangle_c - \beta\langle S^{a,u}_i S^{b,v}_j H_H\rangle_c + \ldots \quad \text{(B4)}$$

For both Heisenberg and Ising Hamiltonians, any nonzero contribution to the correlation function must have an even

number of spin components per site [i.e., $(S_i^{a,u})^2$]. The zeroth-order term in β is obtained trivially,

$$\langle S_i^{a,u} S_j^{b,v} \rangle_c = \langle S_i^{a,u} S_j^{b,v} \rangle_o = (1/n)\,\delta_{i,j}\delta^{a,b}\delta^{u,v},$$

The first-order contribution has two terms in the cumulant,

$$\langle S_i^{a,u} S_j^{b,v} H \rangle_c = \langle S_i^{a,u} S_j^{b,v} H \rangle_o - \langle S_i^{a,u} S_j^{b,v} \rangle_o \langle H \rangle_o,$$

but the second does not contribute because $\langle H \rangle_o \propto \langle S_l^{\tilde{a},\tilde{u}} S_m^{\tilde{b},\tilde{v}} \rangle_o = 0$, spins in the Hamiltonian can not be at the same site. The first term yields the result

$$\langle S_i^{a,u} S_j^{b,v} H \rangle_o = -\tfrac{1}{2} \sum_{l,m} \sum_{\tilde{a},\tilde{b}} \sum_{\tilde{u},\tilde{v}} \mathcal{J}_{\tilde{u}\tilde{v}}^{\tilde{a}\tilde{b}}(i,j) \langle S_i^{a,u} S_j^{b,v} S_l^{\tilde{a},\tilde{u}} S_m^{\tilde{b},\tilde{v}} \rangle$$
$$= -(1/n^2)\mathcal{J}_{uv}^{ab}(i,j). \tag{B5}$$

Therefore, Eq. (B4) can be rewritten as

$$\langle S_i^{a,u} S_j^{b,v} \rangle \approx (1/n)\,\delta_{i,j}\delta^{a,b}\delta^{u,v} + (\beta/n^2)\mathcal{J}_{uv}^{ab}(i,j). \tag{B6}$$

We obtain an expression for the scattering cross section by substituting the result of Eq. (B6) into Eq. (B2), and then that result into Eq. (11); we use the identity $\mathbf{Q}=\mathbf{q}+\mathbf{G}$ and the definition of the Fourier transform of $\mathcal{J}_{uv}^{ab}(i,j)$, Eq. (8), to arrive at

$$\frac{1}{N_{\text{cell}}}\frac{d\sigma(Q)}{d\Omega} = (C/n)[f(Q)]^2 \sum_{a,b} \sum_{u,v} (\hat{n}_\perp^u \cdot \hat{n}_\perp^v) \times \left(\delta^{a,b}\delta^{u,v} + \frac{\beta}{n}\mathcal{J}_{uv}^{ab}(-\mathbf{q}) \right) e^{\imath \mathbf{G}\cdot\mathbf{r}^{ab}}, \tag{B7}$$

where C is a constant. Note, a factor of $1/N_{\text{cell}}$ has been absorbed into the expression of the Fourier transform of the correlation function, Eq. (B6), in order to remain consistent with our use of Eq. (A23) in the derivation of the mean-field neutron-scattering cross-section, Eq. (A37). The interaction matrix, $\mathcal{J}_{uv}^{ab}(-\mathbf{q})$, in Eq. (B7) is not diagonal. In order to calculate the differential cross section for the pyrochlore lattice, or any lattice with a basis, we must diagonalize $\mathcal{J}_{uv}^{ab}(-\mathbf{q})$. This is done with unitary matrix $U(\mathbf{q})$, or $U_{u,\mu}^{a,\alpha}(\mathbf{q})$ in component form. The first term on the right-hand side of Eq. (B7) follows directly from the definition of $U(\mathbf{q})$,

$$\sum_{\alpha,\mu} U_{u,\mu}^{a,\alpha}(-\mathbf{q}) U_{\mu,v}^{\alpha,b}(\mathbf{q}) = \mathbf{I} = \delta^{a,b}\delta^{u,v}, \tag{B8}$$

where $\mathbf{I}$ is the appropriate identity matrix. The transformation of the second term uses Eq. (A25) and solves for $\mathcal{J}(\mathbf{q})$,

$$\mathcal{J}(\mathbf{q}) = U(\mathbf{q})\lambda(\mathbf{q})U^\dagger(\mathbf{q}),$$

or in component form,

$$\mathcal{J}_{uv}^{ab}(-\mathbf{q}) = \sum_{\alpha,\mu} \lambda_\mu^\alpha(\mathbf{q}) U_{u,\mu}^{a,\alpha}(-\mathbf{q}) U_{\mu,v}^{\alpha,b}(\mathbf{q}), \tag{B9}$$

where $\lambda_\mu^\alpha(-\mathbf{q}) = \lambda_\mu^\alpha(\mathbf{q})$. Using the results from Eqs. (B8) and (B9), the expression for the scattering cross section becomes

$$\frac{1}{N_{\text{cell}}}\frac{d\sigma(Q)}{d\Omega} = (C/n)[f(Q)]^2 \sum_{\alpha,\mu} \sum_{a,b} \sum_{u,v} (\hat{n}_\perp^u \cdot \hat{n}_\perp^v) \times \left(1 + \frac{\beta}{n}\lambda_\mu^\alpha(\mathbf{q}) \right) U_{u,\mu}^{a,\alpha}(-\mathbf{q}) U_{\mu,v}^{\alpha,b}(\mathbf{q}) e^{\imath \mathbf{G}\cdot\mathbf{r}^{ab}}. \tag{B10}$$

In the high-temperature limit ($\beta \to 0$), one can write

$$\left(1 + \frac{\beta}{n}\lambda_\mu^\alpha(\mathbf{q}) \right) \approx \left(1 - \frac{\beta}{n}\lambda_\mu^\alpha(\mathbf{q}) \right)^{-1},$$

and the mean-field result is recovered,

$$\frac{1}{N_{\text{cell}}}\frac{d\sigma(Q)}{d\Omega} = C[f(Q)]^2 \sum_{\alpha,\mu} \frac{|\mathbf{F}_{\mu,\perp}^\alpha(\mathbf{q})|^2}{(n - \beta\lambda_\mu^\alpha(\mathbf{q}))}, \tag{B11}$$

where $\mathbf{F}_{\mu,\perp}^\alpha(\mathbf{q})$ is given by Eq. (A36) with $U_{u,\mu}^{a,\alpha}(-\mathbf{q}) = U_{\mu,u}^{\alpha,a}(\mathbf{q})$. For a $\langle 111 \rangle$ Ising model, the indices (u,v) and (μ,ν) are dropped from our presentation, $n=1$, and $\mathbf{F}_\perp^\alpha(\mathbf{q})$ is given by Eq. (A39).

APPENDIX C: EWALD EQUATIONS

Here we treat the dipole-dipole term in $\mathcal{J}(\mathbf{q})$ via the Ewald method.[75] In MFT one works in the thermodynamic limit, so one has an infinite lattice sum. Within the Ewald approach, one recasts this infinite and conditionally convergent series as two finite absolutely convergent (rapidly converging) sums.[58,76] The application of Ewald's ideas to the Fourier transformed dipole-dipole interaction is equivalent to the method of long wavelengths presented in Ref. 58.

The general expression of the Fourier transformed dipole-dipole lattice sum is

$$\mathcal{A}(\mathbf{q}) = \sum_i {}' \sum_{\substack{a,b \\ u,v}} \mathcal{A}_{uv}^{ab} e^{-\imath \mathbf{q}\cdot\mathbf{R}_{ij}^{ab}}, \tag{C1}$$

where

$$\mathcal{A}_{uv}^{ab} = \frac{\hat{n}^u \cdot \hat{n}^v}{|\mathbf{R}_{ij}^{ab}|^3} - \frac{3(\hat{n}^u \cdot \mathbf{R}_{ij}^{ab})(\hat{n}^v \cdot \mathbf{R}_{ij}^{ab})}{|\mathbf{R}_{ij}^{ab}|^5}. \tag{C2}$$

The conventions for indices and vectors are described in Section II, and $\mathcal{A}(\mathbf{q})$ is a 12×12 matrix. The sum Σ_i' is over all $\mathbf{R}_{ij}^{ab}$ except the terms $\mathbf{R}_{ij}^{ab}=\mathbf{0}$. To implement the Ewald method, we rewrite Eq. (C2) in the following form:[60]

$$\mathcal{A}_{uv}^{ab} = -(\hat{n}^u \cdot \nabla_x)(\hat{n}^v \cdot \nabla_x) \left\{ \frac{1}{|\mathbf{R}_{ij}^{ab} - \mathbf{x}|} \right\}_{\mathbf{x}=\mathbf{0}}. \tag{C3}$$

Equation (C3) is used in Eq. (C1), and in terms of components one has,

$$\mathcal{A}_{uv}^{ab}(\mathbf{q}) = -(\hat{n}^u \cdot \nabla_x)(\hat{n}^v \cdot \nabla_x) \left\{ \sum_i {}' \frac{e^{-\imath \mathbf{q}\cdot\mathbf{R}_{ij}^{ab}}}{|\mathbf{R}_{ij}^{ab} - \mathbf{x}|} \right\}_{\mathbf{x}=\mathbf{0}}. \tag{C4}$$

The goal of the Ewald method is to rewrite Eq. (C4), a conditionally convergent series, as two absolutely convergent series, one in real space and the other in reciprocal space

(*k*-space). We begin by writing the sum inside the brackets as a sum over all $\mathbf{R}_{ij}^{ab}$, the result is

$$\mathcal{A}_{uv}^{ab}(\mathbf{q}) = -(\hat{n}^u\cdot\nabla_x)(\hat{n}^v\cdot\nabla_x)\left\{\sum_i \frac{e^{-\imath\mathbf{q}\cdot\mathbf{R}_{ij}^{ab}}}{|\mathbf{R}_{ij}^{ab}-\mathbf{x}|}\right\}_{\mathbf{x}=\mathbf{0}} + \delta^{ab}(\hat{n}^u\cdot\nabla_x)(\hat{n}^v\cdot\nabla_x)\left\{\frac{1}{|\mathbf{x}|}\right\}_{\mathbf{x}=\mathbf{0}}. \tag{C5}$$

Next, the definition of a Gaussian integral (also a gamma function identity[77]),

$$\frac{1}{|\mathbf{R}|} = \frac{2}{\sqrt{\pi}}\int_0^\infty e^{-t^2R^2}dt,$$

is used rewrite the point source term, $1/|\mathbf{R}_{ij}^{ab}-\mathbf{x}|$, in Eq. (C5). The Fourier-transformed dipole-dipole lattice sum now reads

$$\mathcal{A}_{uv}^{ab}(\mathbf{q}) = -(\hat{n}^u\cdot\nabla_x)(\hat{n}^v\cdot\nabla_x)\int_0^\infty dt\frac{2}{\sqrt{\pi}}e^{-\imath\mathbf{q}\cdot\mathbf{x}} \times\left\{\sum_i e^{-t^2|\mathbf{R}_{ij}^{ab}-\mathbf{x}|^2-\imath\mathbf{q}\cdot(\mathbf{R}_{ij}^{ab}-\mathbf{x})}\right\}_{\mathbf{x}=\mathbf{0}} + \delta^{ab}(\hat{n}^u\cdot\nabla_x)(\hat{n}^v\cdot\nabla_x)\left\{\frac{1}{|\mathbf{x}|}\right\}_{\mathbf{x}=\mathbf{0}}. \tag{C6}$$

The integral in Eq. (C6) is divided into two regions, $[0,\alpha]$ and $[\alpha,\infty)$. It is from this decomposition that the real space ($[\alpha,\infty)$) and *k*-space ($[0,\alpha]$) series will arise. We note that the series resulting from the $[\alpha,\infty)$ integral will have a divergence at $\mathbf{R}_{ij}^{ab}=\mathbf{0}$, hence this term is treated separately. The range of integration is controlled by α; it has units of inverse distance and will play the role of a convergence parameter in the final series. Equation (C6) now reads

$$\mathcal{A}_{uv}^{ab}(\mathbf{q}) = W_{uv}^{ab}(\mathbf{q}) + X_{uv}^{ab}(\mathbf{q}) + Y_{uv}^{ab}, \tag{C7}$$

where

$$W_{uv}^{ab}(\mathbf{q}) = -(\hat{n}^u\cdot\nabla_x)(\hat{n}^v\cdot\nabla_x)\int_0^\alpha dt\frac{2}{\sqrt{\pi}}e^{-\imath\mathbf{q}\cdot\mathbf{x}} \times\left\{\sum_i e^{-t^2|\mathbf{R}_{ij}^{ab}-\mathbf{x}|^2-\imath\mathbf{q}\cdot(\mathbf{R}_{ij}^{ab}-x)}\right\}_{\mathbf{x}=\mathbf{0}}, \tag{C8}$$

$$X_{uv}^{ab}(\mathbf{q}) = -(\hat{n}^u\cdot\nabla_x)(\hat{n}^v\cdot\nabla_x)\int_\alpha^\infty dt\frac{2}{\sqrt{\pi}}e^{-\imath\mathbf{q}\cdot\mathbf{x}} \times\left\{\sum_i{}' e^{-t^2|\mathbf{R}_{ij}^{ab}-\mathbf{x}|^2-\imath\mathbf{q}\cdot(\mathbf{R}_{ij}^{ab}-\mathbf{x})}\right\}_{\mathbf{x}=\mathbf{0}}, \tag{C9}$$

$$Y_{uv}^{ab} = \delta^{ab}(\hat{n}^u\cdot\nabla_x)(\hat{n}^v\cdot\nabla_x)\left\{\frac{1}{|\mathbf{x}|}-\frac{2}{\sqrt{\pi}}\int_\alpha^\infty e^{-t^2|\mathbf{x}|^2}dt\right\}_{\mathbf{x}=\mathbf{0}}. \tag{C10}$$

We treat the expressions for $W_{uv}^{ab}(\mathbf{q})$, $X_{uv}^{ab}(\mathbf{q})$, and Y_{uv}^{ab} in succession.

For $W_{uv}^{ab}(\mathbf{q})$, the sum inside the brackets is a periodic function in $\mathbf{x}$. Therefore, it can be expressed as a Fourier series,

$$f(x) = \sum_i e^{-t^2|\mathbf{R}_{ij}^{ab}-\mathbf{x}|^2-\imath\mathbf{q}\cdot(\mathbf{R}_{ij}^{ab}-\mathbf{x})} = \sum_{\mathbf{k}} g_{\mathbf{k}}e^{\imath\mathbf{k}\cdot\mathbf{x}}. \tag{C11}$$

Solving for $g_{\mathbf{k}}$ one has

$$g_{\mathbf{k}=\mathbf{G}} = \frac{4\pi}{v}\frac{e^{-\imath\mathbf{G}\cdot\mathbf{r}^{ab}}}{|\mathbf{q}-\mathbf{G}|^3}F(z), \tag{C12}$$

where $\mathbf{G}$ is a reciprocal lattice vector, v is the volume of the unit cell,

$$F(z) = \int_0^\infty y\sin(y)e^{-z^2y^2}dy = \frac{\sqrt{\pi}}{4z^3}e^{-1/4z^2}, \tag{C13}$$

and $z=t/|\mathbf{q}-\mathbf{G}|$.[78] One now has the following identity for $f(x)$,

$$f(x) = \sum_i e^{-t^2|\mathbf{R}_{ij}^{ab}-\mathbf{x}|^2-\imath\mathbf{q}\cdot(\mathbf{R}_{ij}^{ab}-\mathbf{x})} = \frac{4\pi}{v}\sum_{\mathbf{G}}\frac{e^{-\imath\mathbf{G}\cdot(\mathbf{r}^{ab}-\mathbf{x})}}{|\mathbf{q}-\mathbf{G}|^3}F(z). \tag{C14}$$

Substituting Eq. (C14) into Eq. (C8), differentiating, and imposing the limit on $\mathbf{x}$ yields

$$W_{uv}^{ab}(\mathbf{q}) = \frac{4\pi}{v}\sum_{\mathbf{G}}\frac{[\hat{n}^u\cdot(\mathbf{q}-\mathbf{G})][\hat{n}^v\cdot(\mathbf{q}-\mathbf{G})]}{|\mathbf{q}-\mathbf{G}|^3}e^{-\imath\mathbf{G}\cdot\mathbf{r}^{ab}} \times\frac{2}{\sqrt{\pi}}\int_0^\alpha dtF(t/|\mathbf{q}-\mathbf{G}|). \tag{C15}$$

The integral over $[0,\alpha]$ is readily performed by using the result from Eq. (C13). Therefore, the reciprocal space sum in the Ewald decomposition reads

$$W_{uv}^{ab}(\mathbf{q}) = \frac{4\pi}{v}\sum_{\mathbf{G}}\frac{[\hat{n}^u\cdot(\mathbf{q}-\mathbf{G})][\hat{n}^v\cdot(\mathbf{q}-\mathbf{G})]}{|\mathbf{q}-\mathbf{G}|^2} \times e^{-|\mathbf{q}-\mathbf{G}|^2/4\alpha^2}e^{-\imath\mathbf{G}\cdot\mathbf{r}^{ab}}, \tag{C16}$$

where the sum is over all reciprocal lattice vectors $\mathbf{G}$. We note, however, the series for $W_{uv}^{ab}(\mathbf{q})$ has a nonanalytic term at $\mathbf{G}=\mathbf{0}$ when at the zone center, $\mathbf{q}=\mathbf{0}$. This point is discussed below.

The expression for $X_{uv}^{ab}(\mathbf{q})$, Eq. (C9), can be rearranged to obtain an identifiable integral. By reversing the sum and integral in Eq. (C9), we obtain

$$X_{uv}^{ab}(\mathbf{q}) = -(\hat{n}^u\cdot\nabla_x)(\hat{n}^v\cdot\nabla_x)\sum_i{}' e^{-\imath\mathbf{q}\cdot\mathbf{R}_{ij}^{ab}} \times\frac{2}{\sqrt{\pi}}\int_\alpha^\infty dt\, e^{-t^2|\mathbf{R}_{ij}^{ab}-\mathbf{x}|^2}\big|_{\mathbf{x}=0}. \tag{C17}$$

The integral in Eq. (C17) can be expressed as a complementary error function,[77]

$$\mathrm{erfc}(z) = \frac{2}{\sqrt{\pi}}\int_z^\infty e^{-x^2}dx.$$

A final form for $X_{uv}^{ab}(\mathbf{q})$ is obtained by first applying the differential operators in Eq. (C17), followed by taking the limit $\mathbf{x}\to 0$, and then integrating to get

$$X^{ab}_{uv}(\mathbf{q}) = \sum_i {}' [S1^{ab}_{uv}(\mathbf{R}^{ab}_{ij}) - S2^{ab}_{uv}(\mathbf{R}^{ab}_{ij})] e^{-\imath \mathbf{q}\cdot\mathbf{R}^{ab}_{ij}}, \quad \text{(C18)}$$

where

$$S1^{ab}_{uv}(\mathbf{R}^{ab}_{ij}) = (\hat{n}^u \cdot \hat{n}^v) \left\{ \frac{2\alpha}{\sqrt{\pi}} \frac{e^{-\alpha^2 |\mathbf{R}^{ab}_{ij}|^2}}{|\mathbf{R}^{ab}_{ij}|^2} + \frac{\mathrm{erfc}(\alpha |\mathbf{R}^{ab}_{ij}|)}{|\mathbf{R}^{ab}_{ij}|^3} \right\}, \quad \text{(C19)}$$

$$S2^{ab}_{uv}(\mathbf{R}^{ab}_{ij}) = (\hat{n}^u \cdot \mathbf{R}^{ab}_{ij})(\hat{n}^v \cdot \mathbf{R}^{ab}_{ij}) \times \left\{ \left[\frac{4\alpha^3}{\sqrt{\pi} |\mathbf{R}^{ab}_{ij}|^2} + \frac{6\alpha}{\sqrt{\pi} |\mathbf{R}^{ab}_{ij}|^4} \right] e^{-\alpha^2 |\mathbf{R}^{ab}_{ij}|^2} + \frac{3\,\mathrm{erfc}(\alpha |\mathbf{R}^{ab}_{ij}|)}{|\mathbf{R}^{ab}_{ij}|^5} \right\}. \quad \text{(C20)}$$

Equations (C18)–(C20) form the real-space sum in the Ewald decomposition of the dipole-dipole interaction. Note that the sum in Eq. (C18) is over all Bravais lattice displacement vectors $\mathbf{R}_{ij}$, with j fixed, except $\mathbf{R}_{ij}=\mathbf{0}$. Hence, the real-space Ewald series is analytic everywhere.

In treating the singular terms in Eq. (C10), one applies differential operators first to get

$$Y^{ab}_{uv} = \lim_{\mathbf{x}\to\mathbf{0}} \delta^{ab} \left\{ - \frac{(\hat{n}^u \cdot \hat{n}^v)}{|\mathbf{x}|^3} + \frac{3(\hat{n}^u \cdot \mathbf{x})(\hat{n}^v \cdot \mathbf{x})}{|\mathbf{x}|^5} + (S1^{ab}_{uv}(\mathbf{x}) - S2^{ab}_{uv}(\mathbf{x})) \right\}, \quad \text{(C21)}$$

where $S1^{ab}_{uv}(\mathbf{x})$ and $S2^{ab}_{uv}(\mathbf{x})$ are given by Eqs. (C19) and (C20), respectively, with $\mathbf{R}^{ab}_{ij}$ replaced by $\mathbf{x}$. To evaluate the limit in Eq. (C21), one expands the exponential function to $O(\mathbf{x}^2)$ and the complementary error function to order $O(\mathbf{x}^3)$. The result is the constant,

$$Y^{ab}_{uv} = - \frac{4\alpha^3}{3\sqrt{\pi}} (\hat{n}^u \cdot \hat{n}^v) \delta^{a,b}. \quad \text{(C22)}$$

Collecting the results of Eqs. (C16), (C18)–(C20), and (C22), we write the Ewald representation of the **q**-dependent dipole-dipole interaction as

$$\mathcal{A}^{ab}_{uv}(\mathbf{q}) = - \frac{4\alpha^3}{3\sqrt{\pi}} (\hat{n}^u \cdot \hat{n}^v) \delta^{a,b} + \frac{4\pi}{v} \sum_{\mathbf{G}} K_{uv}(\mathbf{q}-\mathbf{G}) e^{-|\mathbf{q}-\mathbf{G}|^2/4\alpha^2} e^{-\imath \mathbf{G}\cdot\mathbf{r}^{ab}} + \sum_i {}' [S1^{ab}_{uv}(\mathbf{R}^{ab}_{ij}) - S2^{ab}_{uv}(\mathbf{R}^{ab}_{ij})] e^{-\imath \mathbf{q}\cdot\mathbf{R}^{ab}_{ij}}, \quad \text{(C23)}$$

where

$$K_{uv}(\mathbf{q}-\mathbf{G}) = \frac{[\hat{n}^u \cdot (\mathbf{q}-\mathbf{G})][\hat{n}^v \cdot (\mathbf{q}-\mathbf{G})]}{|\mathbf{q}-\mathbf{G}|^2}. \quad \text{(C24)}$$

In our derivation of the Ewald equations there is no reference to a specific lattice structure. Therefore, the Ewald results encapsulated in Eq. (C23) hold for any lattice described by a set of translation vectors $\{\mathbf{R}^{ab}_{ij}\}$. Through the unit vectors $\hat{n}^u$ (where local quantization axes can be treated by including a sublattice index, i.e., $\hat{n}^{a,u}$), the freedom to define the spin symmetry (e.g., Heisenberg, XY, Ising) has been ensured, too. For the work discussed in this article, we consider both Heisenberg and ⟨111⟩ Ising spins on the pyrochlore lattice. For Heisenberg spins, $\mathcal{A}^{ab}_{uv}(\mathbf{q})$ is calculated for all sublattices (a,b) and spin components (u,v), the resulting $\mathcal{A}(\mathbf{q})$ is a 12×12 symmetric matrix contribution to $\mathcal{J}(\mathbf{q})$. For ⟨111⟩ Ising spins, the sums over spin components are dropped and the local quantization vectors are substituted, $\hat{z}^a$. One calculates $\mathcal{A}^{ab}(\mathbf{q})$ for all sublattices (a,b), resulting in $\mathcal{A}(\mathbf{q})$ a symmetric 4×4 contribution to $\mathcal{J}(\mathbf{q})$. For each pyrochlore model, $\mathcal{A}(\mathbf{q})$ is determined at every **q**-point in a mesh that covers the first Brillouin zone in the (hhl) plane. These matrices are stored and then used in the formation of $\mathcal{J}(\mathbf{q})$ to calculate the neutron-scattering cross section, Eq. (16) or Eq. (18), for a specified set of interaction parameters (i.e., J, D, Δ, T). Because $\mathcal{A}(\mathbf{q})$ is calculated only for **q** in the first zone, the term $\mathcal{K}_{uv}(\mathbf{q}-\mathbf{G})$ in Eq. (C23) is ill defined at $\mathbf{q}=\mathbf{G}=0$. We discuss the small **q** behavior of the Ewald equations below.

The parameter α used to divide the integral in Eq. (C6) functions as a convergence parameter in the Ewald sums, Eq. (C23). Although, the result of $\mathcal{A}^{ab}_{uv}(\mathbf{q})$ is independent of the value of α, in practice one chooses α so that both real and reciprocal sums converge rapidly. Note that the convergence of the real-space sum, Eqs. (C18)–(C20), is enhanced by a large value for α, while the convergence of the reciprocal sum, Eq. (C16), is improved for a small α. In choosing a convergence parameter, we followed Ref. 59 and set $\alpha = \sqrt{\pi}/v$, where v is the volume of the unit cell. For a pyrochlore lattice defined in the rhombohedral basis with a cubic cell size of $\overline{a}$, we used $v=\overline{a}^3/4$. The real- and reciprocal-space sums converged at about the same rate for this value of α. We obtained similar results for $\mathcal{A}^{ab}_{uv}(\mathbf{q})$ using $\alpha=\sqrt{\pi/2v}$ and $\alpha=\sqrt{2\pi/v}$. Our Ewald results were checked by comparing the maximum eigenvalues of $\mathcal{A}(\mathbf{q})$ to those generated from a direct lattice sum of $\mathcal{A}(\mathbf{q})$ out to some cutoff distance r_c. Comparisons were done for the bcc and fcc lattices. We also performed tests of our Ewald equations for the pyrochlore lattice by calculating the soft-mode spectrum of $\mathcal{A}(\mathbf{q})$ in the spin-ice regime, e.g., $D=1$. Ewald results along $(00l)$ in the first Brillouin zone were compared to calculations with the dipolar sum cutoff at different maximum separation distances r_c. The cutoff-results approach the Ewald results as r_c increases. This spectrum of eigenvalues agrees well with the spectrum generated from a direct lattice sum for $\mathcal{A}(\mathbf{q})$ with a cutoff distance of $r_c=1000$, Fig. 6 in Ref. 79. The Ewald method eliminates the ripples in the soft-mode spectrum of $\mathcal{A}(\mathbf{q})$ by effectively taking the range of interaction to infinity.

The reciprocal space sum in Eq. (C23) has a nonanalytic term at the point $\mathbf{q}=\mathbf{0}$ in the first Brillouin zone. If we consider the $\mathbf{G}=\mathbf{0}$ contribution to Eq. (C16), we have,

$$W^{ab}_{uv}(\mathbf{q}, \mathbf{G}=\mathbf{0}) = \frac{4\pi}{v} \frac{(\hat{n}^u \cdot \mathbf{q})(\hat{n}^v \cdot \mathbf{q})}{|\mathbf{q}|^2} e^{-|\mathbf{q}|^2/4\alpha^2}. \quad \text{(C25)}$$

In the limit of small **q** the exponential is expanded to yield

$$W_{uv}^{ab}(\mathbf{q},\mathbf{G}=\mathbf{0}) \approx \frac{4\pi}{v}\frac{(\hat{n}^u\cdot\mathbf{q})(\hat{n}^v\cdot\mathbf{q})}{|\mathbf{q}|^2}\left(1-\frac{|\mathbf{q}|^2}{4\alpha^2}\right), \quad \text{(C26)}$$

where in the limit $\mathbf{q}\to\mathbf{0}$ the value of

$$\frac{4\pi}{v}\frac{(\hat{n}^u\cdot\mathbf{q})(\hat{n}^v\cdot\mathbf{q})}{|\mathbf{q}|^2}$$

depends on the direction in which one approaches the zone center. The nonanalytic term can be related to the macroscopic field of the dipoles and is shape dependent (see Section 30 in Ref. 58). We drop this term from our calculation to obtain a completely smooth spectrum all the way to $\mathbf{q}=0,0,0$. The physics of spin ice is not affected by this omission because all modes contribute to the PM scattering with $\mathbf{q}=0,0,1$ going critical at T_c^{MF}. The case of $Tb_2Ti_2O_7$ is more subtle because it is the $\mathbf{q}=0,0,0$ soft mode that goes critical. However, our focus here is not the ordered state of $Tb_2Ti_2O_7$, where a $\mathbf{q}=\mathbf{0}$ ordered state is expected for a pyrochlore AFM with either $\langle 111\rangle$ Ising[25,28,35] or Heisenberg[5] spins. Instead, we are concerned with understanding the physics in the paramagnetic regime of this system as a first step toward unraveling the mystery surrounding the failure of $Tb_2Ti_2O_7$ to order at 50 mK.

APPENDIX D: SYMMETRY EXCLUDED SCATTERING

The paramagnetic neutron scattering spectrum of $Tb_2Ti_2O_7$ in the (hhl) plane contains a strong but broad region of intensity about $\mathbf{Q}=0,0,2$ with no discernible correlations near the zone center, $\mathbf{Q}=0,0,0$.[41] In this appendix, we put forward arguments based only on the structure of the lattice and the symmetry of spin space to demonstrate that the PM scattering intensity profile described above can not be realized by $\langle 111\rangle$ Ising spins on the pyrochlore lattice, but is allowed if the spins are Heisenberg-like.

For the Ising pyrochlores, the map of scattering intensity is determined by the function $\mathbf{F}_\perp^\alpha(\mathbf{q})$, Eq. (19), which contains only information on the symmetry of the lattice through the eigenvectors $U^{a,\alpha}(\mathbf{q})$ and the phase-factor $\exp(\imath\mathbf{G}\cdot r^a)$ and the symmetry of spin space through the local quantization axis $\mathbf{z}^a$. We consider a unit tetrahedron with scattering vectors $\mathbf{Q}$ restricted to the $(00l)$ direction. To handle the situation near the origin, we express all $\mathbf{Q}$ as a small displacement from a reciprocal lattice vector (i.e., $\mathbf{Q}=\mathbf{G}+\mathbf{q}=0,0,\ell+0,0,\delta$), where $0<\delta<1$, ℓ is an integer, and a factor of $2\pi/\overline{a}$ is implied. The term $0,0,\delta$ falls in the first zone and, therefore, determines the eigenvalues and eigenvectors. Using the values for $\mathbf{r}^a$ and $\hat{z}^a$ defined in Table I we write

$$\mathbf{F}_\perp^\alpha(0,0,\ell+\delta)=\frac{(1,1,0)}{\sqrt{3}}[U^{1,\alpha}(\delta)-U^{2,\alpha}(\delta)] + \frac{(1,-1,0)}{\sqrt{3}}[U^{4,\alpha}(\delta)-U^{3,\alpha}(\delta)]e^{\imath(\ell\pi/2)}. \quad \text{(D1)}$$

Note that the projections of the spins onto the plane perpendicular to the direction of $\mathbf{Q}$ sum to zero (i.e., $\hat{z}_\perp^{(1)}+\hat{z}_\perp^{(2)}+\hat{z}_\perp^{(3)}+\hat{z}_\perp^{(4)}=0$). For wave vectors $\mathbf{Q}=0,0,\delta$ and $\mathbf{Q}=0,0,2+\delta$, one has the following:

$$\mathbf{F}_\perp^\alpha(0,0,\delta)=\frac{(1,1,0)}{\sqrt{3}}[U^{1,\alpha}(\delta)-U^{2,\alpha}(\delta)] + \frac{(1,-1,0)}{\sqrt{3}}[U^{4,\alpha}(\delta)-U^{3,\alpha}(\delta)] \quad \text{(D2)}$$

and

$$\mathbf{F}_\perp^\alpha(0,0,2+\delta)=\frac{(1,1,0)}{\sqrt{3}}[U^{1,\alpha}(\delta)-U^{2,\alpha}(\delta)] - \frac{(1,-1,0)}{\sqrt{3}}[U^{4,\alpha}(\delta)-U^{3,\alpha}(\delta)]. \quad \text{(D3)}$$

The modulus squared of these two functions, e.g., the numerator of the scattering cross section, yields the same numerical result,

$$\begin{aligned}|\mathbf{F}_\perp^\alpha(0,0,\delta)|^2 &= |\mathbf{F}_\perp^\alpha(0,0,2+\delta)|^2\\ &= \tfrac{1}{3}\{[U^{1,\alpha}(\delta)-U^{2,\alpha}(\delta)-U^{3,\alpha}(\delta)+U^{4,\alpha}(\delta)]^2\\ &\quad +[U^{1,\alpha}(\delta)-U^{2,\alpha}(\delta)+U^{3,\alpha}(\delta)-U^{4,\alpha}(\delta)]^2\}.\end{aligned}$$

This means the scattering cross section, given by Eq. (18), in the limit $\delta\to 0$, is the same (or exactly correlated) for $\mathbf{Q}=0,0,0$ and $\mathbf{Q}=0,0,2$, absent the magnetic form factor $(f(Q))$. Therefore, the paramagnetic scattering of $Tb_2Ti_2O_7$ cannot be generated by a model with Ising spins (infinite local $\langle 111\rangle$ anisotropy).

In the case of Heisenberg spins with finite single-ion anisotropy, we consider the function $\mathbf{F}_{\mu,\perp}^\alpha(\mathbf{q})$ is given by Eq. (17). Again, restricting ourselves to wave vectors along the $(00l)$ direction, we have the general result

$$\mathbf{F}_{\mu,\perp}^\alpha(0,0,\ell+\delta)=\mathbf{U}_{\mu,\perp}^{1,\alpha}(\delta)+\mathbf{U}_{\mu,\perp}^{2,\alpha}(\delta) + [\mathbf{U}_{\mu,\perp}^{3,\alpha}(\delta)+\mathbf{U}_{\mu,\perp}^{4,\alpha}(\delta)]e^{\imath(\ell\pi/2)}, \quad \text{(D4)}$$

where $\mathbf{U}_{\mu,\perp}^{a,\alpha}(\delta)=[U_{x,\mu}^{a,\alpha}(\delta),U_{y,\mu}^{a,\alpha}(\delta),0]$. For $\mathbf{Q}$ near 0,0,0 and 0,0,2, we obtain the following two forms:

$$\mathbf{F}_{\mu,\perp}^\alpha(0,0,\delta)=\mathbf{U}_{\mu,\perp}^{1,\alpha}(\delta)+\mathbf{U}_{\mu,\perp}^{2,\alpha}(\delta)+\mathbf{U}_{\mu,\perp}^{3,\alpha}(\delta)+\mathbf{U}_{\mu,\perp}^{4,\alpha}(\delta) \quad \text{(D5)}$$

and

$$\mathbf{F}_{\mu,\perp}^\alpha(0,0,2+\delta)=\mathbf{U}_{\mu,\perp}^{1,\alpha}(\delta)+\mathbf{U}_{\mu,\perp}^{2,\alpha}(\delta)-[\mathbf{U}_{\mu,\perp}^{3,\alpha}(\delta)+\mathbf{U}_{\mu,\perp}^{4,\alpha}(\delta)]. \quad \text{(D6)}$$

Taking the modulus squared we get

$$|\mathbf{F}_\perp^{\alpha,\mu}(0,0,\delta)|^2=(A^2+B^2)+(C^2+D^2)+2(AC+BD) \quad \text{(D7)}$$

and

$$|\mathbf{F}_\perp^{\alpha,\mu}(0,0,2+\delta)|^2=(A^2+B^2)+(C^2+D^2)-2(AC+BD), \quad \text{(D8)}$$

where

$$A = U^{1,\alpha}_{x,\mu}(\delta) + U^{2,\alpha}_{x,\mu}(\delta),$$

$$B = U^{1,\alpha}_{y,\mu}(\delta) + U^{2,\alpha}_{y,\mu}(\delta),$$

$$C = U^{3,\alpha}_{x,\mu}(\delta) + U^{4,\alpha}_{x,\mu}(\delta),$$

$$D = U^{3,\alpha}_{y,\mu}(\delta) + U^{4,\alpha}_{y,\mu}(\delta). \quad \text{(D9)}$$

Equations (D7) and (D8) are not strictly equivalent. Hence, it is possible to have paramagnetic spin-spin correlations about $\mathbf{Q}=0,0,2$ while intensity about $\mathbf{Q}=0,0,0$ is suppressed. This result puts on a firm theoretical footing the need to describe $Tb_2Ti_2O_7$ by a three-component Heisenberg model with finite anisotropy.

*Current address: Department of Physics, Southern Connecticut State University, 501 Crescent Street, New Haven, CT 06515. Electronic address: enjalran@gandalf.uwaterloo.ca

†Electronic address: gingras@gandalf.uwaterloo.ca

[1] A. P. Ramirez, Annu. Rev. Mater. Sci. **24**, 453 (1994).

[2] J. E. Greedan, J. Mater. Chem. **11**, 37 (2001).

[3] S. T. Bramwell and M. J. P. Gingras, Science **294**, 1495 (2001).

[4] N. P. Raju, M. Dion, M. J. P. Gingras, T. E. Mason, and J. E. Greedan, Phys. Rev. B **59**, 14 489 (1999).

[5] S. E. Palmer and J. T. Chalker, Phys. Rev. B **62**, 488 (2000).

[6] J. D. M. Champion, A. S. Wills, T. Fennell, S. T. Bramwell, J. S. Gardner, and M. A. Green, Phys. Rev. B **64**, 140407 (2001).

[7] S. R. Dunsiger, R. F. Kiefl, K. H. Chow, B. D. Gaulin, M. J. P. Gingras, J. E. Greedan, A. Keren, K. Kojima, G. M. Luke, W. A. MacFarlane, N. P. Raju, J. E. Sonier, Y. J. Uemura, and W. D. Wu, Phys. Rev. B **54**, 9019 (1996).

[8] M. J. P. Gingras, C. V. Stager, N. P. Raju, B. D. Gaulin, and J. E. Greedan, Phys. Rev. Lett. **78**, 947 (1997).

[9] J. S. Gardner, B. D. Gaulin, S.-H. Lee, C. Broholm, N. P. Raju, and J. E. Greedan, Phys. Rev. Lett. **83**, 211 (1999).

[10] B. D. Gaulin, J. N. Reimers, T. E. Mason, J. E. Greedan, and Z. Tun, Phys. Rev. Lett. **69**, 3244 (1992).

[11] J. N. Reimers, J. E. Greedan, R. K. Kremer, E. Gmelin, and M. A. Subramanian, Phys. Rev. B **43**, 3387 (1991).

[12] M. J. Harris, S. T. Bramwell, D. F. McMorrow, T. Zeiske, and K. W. Godfrey, Phys. Rev. Lett. **79**, 2554 (1997).

[13] A. P. Ramirez, A. Hayashi, R. J. Cava, R. Siddharthan, and B. S. Shastry, Nature (London) **399**, 333 (1999).

[14] B. S. Shastry, Physica B **329–333**, 1024 (2003).

[15] J. S. Gardner, S. R. Dunsiger, B. D. Gaulin, M. J. P. Gingras, J. E. Greedan, R. F. Kiefl, M. D. Lumsden, W. A. MacFarlane, N. P. Raju, J. E. Sonier, I. Swainson, and Z. Tun, Phys. Rev. Lett. **82**, 1012 (1999).

[16] J. S. Gardner, A. Keren, G. Ehlers, E. Segal, J. M. Roper, B. Føak, M. B. Stone, P. R. Hammar, D. H. Reich, and B. D. Gaulin, Phys. Rev. B **68**, 180401(R) (2003).

[17] Y. Taguchi, Y. Oohara, H. Yoshizawa, N. Nagaosa, and Y. Tokura, Science **291**, 2573 (2001).

[18] D. Yanagishima and Y. Maeno, J. Photogr. Sci. **70**, 2880 (2001).

[19] M. Hanawa, Y. Muraoka, T. Tayama, T. Sakakibara, J. Yamaura, and Z. Hiroi, Phys. Rev. Lett. **87**, 187001 (2001).

[20] H. Sakai, K. Yoshimura, H. Ohno, H. Kato, S. Kambe, R. E. Walstedt, T. D. Matsuda, and Y. Haga, J. Phys.: Condens. Matter **13**, L785 (2001).

[21] S. Kondo, D. C. Johnston, C. A. Swenson, F. Borsa, A. V. Mahajan, L. L. Miller, T. Gu, A. I. Goldman, M. B. Maple, D. A. Gajewski, E. J. Freeman, N. R. Dilley, R. P. Dickey, J. Merrin, K. Kojima, G. M. Luke, Y. J. Uemura, O. Chmaissem, and J. D. Jorgensen, Phys. Rev. Lett. **78**, 3729 (1997).

[22] S.-H. Lee, C. Broholm, T. H. Kim, W. Ratcliff, and S.-W. Cheong, Phys. Rev. Lett. **84**, 3718 (2000).

[23] S.-H. Lee, C. Broholm, W. Ratcliff, G. Gasparovic, Q. Huang, T. H. Kim, and S.-W. Cheong, Nature (London) **418**, 856 (2002).

[24] S. Rosenkranz, A. P. Ramirez, A. Hayashi, R. J. Cava, R. Siddharthan, and B. S. Shastry, J. Appl. Phys. **87**, 5914 (2000).

[25] M. J. P. Gingras, B. C. den Hertog, M. Faucher, J. S. Gardner, S. R. Dunsiger, L. J. Chang, B. D. Gaulin, N. P. Raju, and J. E. Greedan, Phys. Rev. B **62**, 6496 (2000).

[26] J. A. Hodges, P. Bonville, A. Forget, A. Yaouanc, P. D. de Réotier, G. André, M. Rams, K. Królas, C. Ritter, P. C. M. Gubbens, C. T. Kaiser, P. J. C. King, and C. Baines, Phys. Rev. Lett. **88**, 077204 (2002).

[27] S. Bramwell and M. J. Harris, J. Phys.: Condens. Matter **10**, L215 (1998).

[28] R. Moessner, Phys. Rev. B **57**, R5587 (1998).

[29] J. D. Bernal and R. H. Fowler, J. Chem. Phys. **1**, 515 (1933).

[30] L. Pauling, J. Am. Chem. Soc. **57**, 2680 (1935).

[31] L. Pauling, *The Nature of the Chemical Bond* (Cornell University Press, Ithaca, NY, 1960).

[32] S. T. Bramwell, M. J. Harris, B. C. den Hertog, M. J. P. Gingras, J. S. Gardner, D. F. McMorrow, A. R. Wildes, A. L. Cornelius, J. D. M. Champion, R. G. Melko, and T. Fennell, Phys. Rev. Lett. **87**, 047205 (2001).

[33] A. L. Cornelius and J. S. Gardner, Phys. Rev. B **64**, 060406 (2001).

[34] S. Bramwell, M. J. P. Gingras, and J. N. Reimers, J. Appl. Phys. **75**, 5523 (1994).

[35] B. C. den Hertog and M. J. P. Gingras, Phys. Rev. Lett. **84**, 3430 (2000).

[36] M. Enjalran, M. J. P. Gingras, Y.-J. Kao, A. G. D. Maestro, and H. R. Molavian, J. Phys.: Condens. Matter **16**, S673 (2004).

[37] G. Luo, S. T. Hess, and L. R. Corruccini, Phys. Lett. A **291**, 306 (2001).

[38] J. Villain, Z. Phys. B **33**, 31 (1979).

[39] J. N. Reimers, A. J. Berlinsky, and A.-C. Shi, Phys. Rev. B **43**, 865 (1991).

[40] R. Moessner and J. T. Chalker, Phys. Rev. Lett. **80**, 2929 (1998).

[41] J. S. Gardner, B. D. Gaulin, A. J. Berlinsky, P. Waldron, S. R Dunsiger, N. P. Raju, and J. E Greedan, Phys. Rev. B **64**, 224416 (2001).

[42] Y. Yasui, M. Kanada, M. Ito, H. Harashina, M. Sato, H. Okumura, K. Kakurai, and H. Kadowaki, J. Phys. Soc. Jpn. **71**, 599 (2002).

[43] I. Mirebeau, I. N. Goncharenko, P. Cadavez-Pares, S. Bramwell,

M. J. P. Gingras, and J. S. Gardner, Nature (London) **420**, 54 (2002).
[44] W. I. Kinney and W. P. Wolf, J. Appl. Phys. **50**, 2115 (1979).
[45] P. Schiffer, A. P. Ramirez, D. A. Huse, and A. J. Valentino, Phys. Rev. Lett. **73**, 2500 (1994).
[46] P. Schiffer, A. P. Ramirez, D. A. Huse, P. L. Gammel, U. Yaron, D. J. Bishop, and A. J. Valentino, Phys. Rev. Lett. **74**, 2379 (1995).
[47] O. A. Petrenko, D. McK. Paul, C. Ritter, T. Zeiske, and M. Yethiraj, Physica B **266**, 41 (1999).
[48] O. A. Petrenko, C. Ritter, M. Yethiraj, and D. McK. Paul, Phys. Rev. Lett. **80**, 4570 (1998).
[49] P. Bonville, J. A. Hodges, J. P. Sanchez, and P. Vulliet, Phys. Rev. Lett. **92**, 167202 (2004).
[50] A. P. Ramirez, B. S. Shastry, A. Hayashi, J. J. Krajewski, D. A. Huse, and R. J. Cava, Phys. Rev. Lett. **89**, 067202 (2002).
[51] J. R. Stewart, G. Ehlers, A. S. Wills, S. T. Bramwell, and J. S. Gardner, J. Phys.: Condens. Matter **16**, L321 (2004).
[52] Y. Yasui, M. Soda, S. Iikubo, M. Ito, M. Sato, N. Hamaguchi, T. Matsushita, N. Wada, T. Takeuchi, N. Aso, and K. Kakura, J. Phys. Soc. Jpn. **72**, 3014 (2003).
[53] A. G. del Maestro and M. J. P. Gingras, J. Phys.: Condens. Matter **16**, 3339 (2004).
[54] P. M. Chaikin and T. C. Lubensky, *Principles of Condensed Matter Physics* (Cambridge University Press, Cambridge, UK, 1995).
[55] A. B. Harris, O. G. Mouritsen, and A. J. Berlinsky, Can. J. Phys. **62**, 915 (1984).
[56] J. N. Reimers, Phys. Rev. B **46**, 193 (1992).
[57] M. Kanada, Y. Yasui, Y. Kondo, S. Iikubo, M. Ito, H. Harashina, M. Sato, H. Okumura, K. Kakurai, and H. Kadowaki, J. Phys. Soc. Jpn. **71**, 313 (2002).
[58] M. Born and K. Huang, *Dynamical Theory of Crystal Lattices* (Oxford University Press, London, 1968).
[59] M. H. Cohen and F. Keffer, Phys. Rev. **99**, 1128 (1955).
[60] A. Aharony and M. E. Fisher, Phys. Rev. B **8**, 3323 (1973).
[61] L. M. Holmes, J. Als-Nielsen, and H. J. Guggenheim, Phys. Rev. B **12**, 180 (1975).
[62] J. Jensen and A. R. MacKintosh, *Rare Earth Magnetism: Structures and Excitations* (Oxford University Press, New York, 1991).
[63] S. Lovesey, *Theory of Neutron Scattering from Condensed Matter, Vol. 2: Polarization Effects and Magnetic Scattering of International Series of Monographs on Physics No. 72* (Oxford University Press, New York, 1984).
[64] R. Moessner and J. T. Chalker, Phys. Rev. B **58**, 12 049 (1998).
[65] B. Canals and D. A. Garanin, Can. J. Phys. **79**, 1323 (2001).
[66] Y.-J. Kao, M. Enjalran, A. D. Maestro, H. R. Molavian, and M. J. P. Gingras, Phys. Rev. B **68**, 172407 (2003).
[67] A. P. Ramirez (private communication).
[68] M. Enjalran and M. J. P. Gingras, cond-mat/0307152 (unpublished).
[69] O. Cépas and B. S. Shastry, Phys. Rev. B **69**, 184402 (2004).
[70] J. R. Stewart, G. Ehlers, A. S. Wills, S. T. Bramwell, and J. S. Gardner, J. Phys.: Condens. Matter **16**, L321 (2004).
[71] S. R. Dunsiger, J. S. Gardner, J. A. Chakhalian, A. L. Cornelius, M. Jaime, R. F. Kiefl, R. Movshovich, W. A. MacFarlane, R. I. Miller, J. E. Sonier, *et al.*, Phys. Rev. Lett. **85**, 3504 (2000).
[72] J. Schweizer, in *Neutron and Synchrotron Radiation for Condensed Matter Studies*, edited by J. Baruchel, J. L. Hodeau, M. S. Lehmann, J. R. Regnard, and C. Schlenker (Springer-Verlag, Berlin, 1994), Vol. II, p. 97.
[73] H. Kadowaki, Y. Ishii, K. Matsuhira, and Y. Hinatsu, Phys. Rev. B **65**, 144421 (2002).
[74] G. S. Rushbrooke, G. A. Baker, and P. J. Wood, *Phase Transitions and Critical Phenomena* (Academic Press, London, 1974), Vol. 3, Chap. Heisenberg Model, p. 245.
[75] P. P. Ewald, Ann. Phys. (Leipzig) **64**, 253 (1921).
[76] S. L. de Leeuw, J. W. Perram, and E. R. Smith, Proc. R. Soc. London, Ser. A **373**, 27 (1980).
[77] G. Arfken, *Mathematical Methods for Physicists*, 3rd ed. (Academic Press, San Diego, 1985).
[78] The result of Eq. (C13) is found in I.S. Gradshteyn, and I. M. Ryzhik, *Table of Integrals, Series, and Products* (Academic Press, San Diego, 1980), Corrected and Enlarged Ed., integral 3.952-1, p. 495.
[79] M. J. P. Gingras and B. C. den Hertog, Can. J. Phys. **79**, 1339 (2001).